

Distribution Agreement

In presenting this thesis as a partial fulfillment of the requirements for a degree from Emory University, I hereby grant to Emory University and its agents the non-exclusive license to archive, make accessible, and display my thesis in whole or in part in all forms of media, now or hereafter now, including display on the World Wide Web. I understand that I may select some access restrictions as part of the online submission of this thesis. I retain all ownership rights to the copyright of the thesis. I also retain the right to use in future works (such as articles or books) all or part of this thesis.

Julia Eisman

April 10, 2018

DNA-based Rolling Motors with Biotin & Streptavidin Brakes

By

Julia Eisman

Dr. Khalid Salaita

Adviser

Department of Chemistry

Dr. Khalid Salaita

Adviser

Dr. José Luis Boigues-Lopez

Committee Member

Dr. Jed Brody

Committee Member

2018

DNA-based Rolling Motors with Biotin & Streptavidin Brakes

By

Julia Eisman

Dr. Khalid Salaita

Adviser

An abstract of
a thesis submitted to the Faculty of Emory College of Arts and Sciences
of Emory University in partial fulfillment
of the requirements of the degree of
Bachelor of Arts with Honors

Department of Physics

2018

Abstract

DNA-based Rolling Motors with Biotin & Streptavidin Brakes

By Julia Eisman

Inspired by biological motors, scientists have produced various molecular machines as model systems including a wide array of DNA walkers. However, another type of machine, DNA rolling motors, are deemed to be favorable in molecular level detection due to their high fidelity and speed. These motors, which roll atop a surface, promise to be the most sensitive and processive DNA machines, but they have yet to be used to detect different proteins. Therefore, in the following experiments, these motors were designed to detect concentrations of streptavidin using biotin as the sensor, and the velocities of DNA particles were measured at different streptavidin concentrations. Following extensive trials, it was found that velocity is, in fact, inversely related to streptavidin concentration lending. This highly sensitive system for detecting streptavidin can be extended to other molecules. Therefore, it offers great possibilities, such as, clinical applications in testing for various diseases. Accurate detection of the presence of such biomolecules has become increasingly important in early diagnosis and, therefore, in increasing survival rates for diseases.

DNA-based Rolling Motors with Biotin & Streptavidin Brakes

By

Julia Eisman

Dr. Khalid Salaita

Adviser

A thesis submitted to the Faculty of Emory College of Arts and Sciences
of Emory University in partial fulfillment
of the requirements of the degree of
Bachelor of Arts with Honors

Department of Physics

2018

Acknowledgements

I would like to express my sincere appreciation to everyone who aided me throughout the process towards accomplishing this thesis. I feel so fortunate to have been given the opportunity to be part of such an incredible and supportive research community.

I would like to thank Dr. Khalid Salaita for providing me support throughout the experimental and writing process. Having not had prior research experience outside of lab classes, this was truly a growing experience and allowed me to realize my passion in research.

I would also like to thank the members of the Salaita lab, in particular Aaron Blanchard and Alisina Bazrafshan, for being so welcoming and patient in answering any questions I had. I have grown so much in my research as a result of all your support and guidance.

Lastly, I would like to thank Dr. José Luis Boigues and Dr. Jed Brody for all of your encouragement and inspiration in pursuing my passion for Spanish and physics during my time at college. I am so grateful you agreed to be on my honors thesis committee.

Table of Contents

1. Introduction	1
2. Experimental Methods	15
2.1. Thermal evaporation of gold films	
2.2. Implementation of wells with IBIDI	
2.3. Fabrication of DNA and biotinylated anchors of varying proportions	
2.4. Backfilling of the surface	
2.5. Hybridization of RNA to DNA anchoring strands	
2.6. Synthesis of azide functionalized particles	
2.7. Production of high density DNA silica particles	
2.8. Synthesis of biotinylated silica particles	
2.9. Addition of varying concentrations of streptavidin to biotinylated particles	
2.10. Preparation of rolling solution and imaging	
2.11. Particle Trajectory Analysis	
2.12. Streptavidin Fluorescence Calibration	
2.13. Testing for non-specific binding of streptavidin using flow cytometry	
3. Results and Discussion	23
4. Conclusion and Future Directions	42
5. References	45

Figures

Figure 1	1
Figure 2	2
Figure 3	3
Figure 4	4
Figure 5	5
Figure 6	6
Figure 7	9
Figure 8	12
Figure 9	24
Figure 10	27
Figure 11	29
Figure 12	32
Figure 13	36
Figure 14	38
Figure 15	39
Figure 16	40
Figure 17	41
Figure 18	44

Tables

Table 1	13
Table 2	25
Table 3	43

1. Introduction

A machine can be described as a system containing several parts, each with a unique function, collectively working together to perform a particular task. A molecular-level machine is composed of a discrete number of molecular components which perform mechanical-like movements in response to certain external stimuli. There are several examples of these machines in biological systems such as the myosin motor, which is responsible for muscle contraction, shown in *Figure 1*.

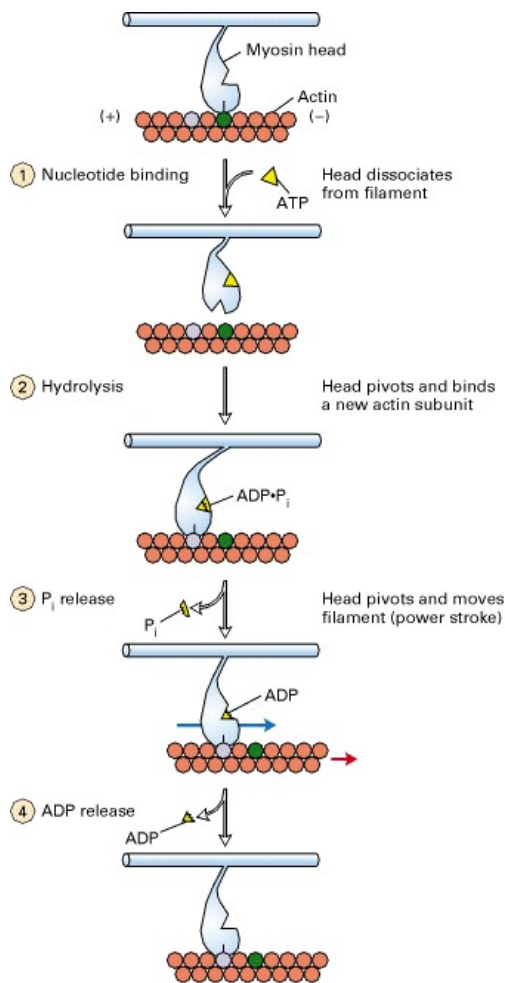


*Figure 1. Myosin thick filaments slide along actin thin filaments to induce muscle contraction.*⁸

Inspired by these molecular machines, scientists have worked on synthetic versions to be useful in numerous applications such as drug delivery and sensing. *Kassem et al.* describes two categories, 'molecular switch' and 'molecular motor', under the broad category of molecular-level machines. Molecular switches are molecular machines whose change in position is dependent on the state of the switch. When the switch is returned to its original state, any mechanical work performed will be reversed as shown in *Figure 2* depicting a nanocar which can traverse a copper track with electrical pulse stimuli (*Sun et al, 2015*).

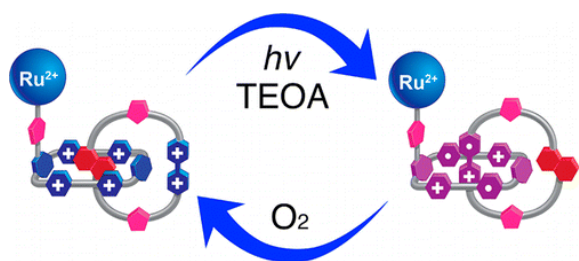


*Figure 2. Nanocar traversing a copper track with electrical pulse stimuli.*¹¹

In contrast, molecular motors are machines in which the change in relative position of the components influences a system as a function of the trajectory of the components. With this function, molecular motors can, in fact, be used to progressively push systems away from equilibrium and maintain continuous directional motion (*Kassem et al., 2017*). An example of these types of molecular machines is depicted in *Figure 3* representing burnt bridge Brownian ratchet which allows the walker to processively move, attaining control of motion against the entropy of random Brownian diffusion (*Bath et al., 2005*).

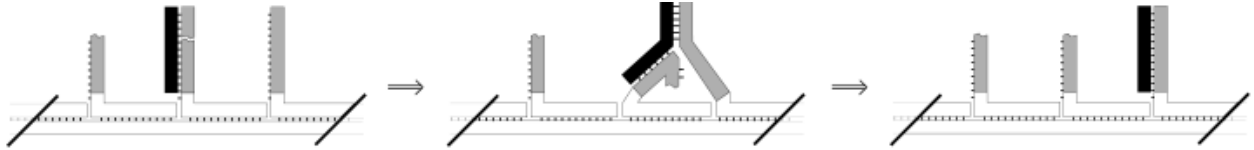


Figure 3. A molecular motor moves a DNA cargo (black strand) along a DNA track. Movement is powered by a nicking enzyme (grey strand), which cleaves itself allowing for the attachment of the next toehold strand. The duplex in the third step forms as it is more stable than that in the second. Damage to the track through this process imposes directionality in a process known as burnt bridge Brownian ratchet.¹

Previous literature comprises the development of more complex versions of the aforementioned molecular motor including various bipedal and multi-pedal DNA walkers, which have been produced to transport cargo along a track. For example, Lund *et al.* developed the molecular spider, illustrated in *Figure 4*, which functions as a multi-pedal walker, the “body” of the machine being a streptavidin molecule with three 8-17 base pair long DNA enzyme “legs.” These projections cleave substrate at an RNA base, allowing it to dissociate and associate with the next substrate (Lund *et al.*, 2010). A major drawback of this system is that the walker’s movement is random as it is driven by Brownian motion, lacking processivity.

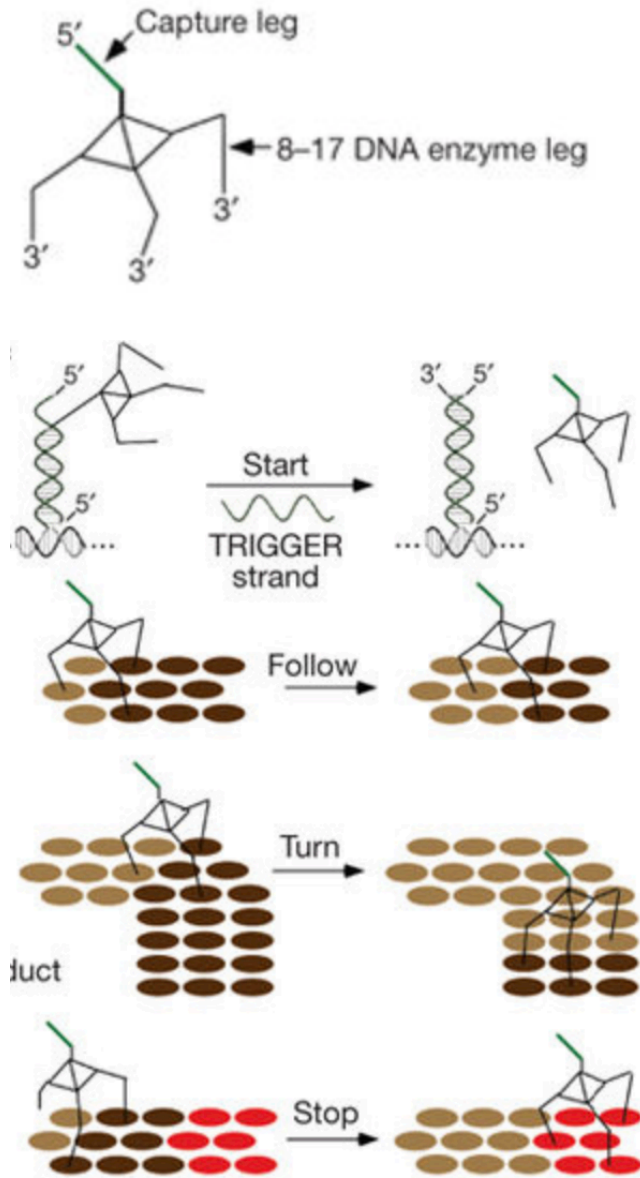


Figure 4. Molecular spider structure and formation upon addition of a trigger strand. The spider has three distinct types of behavior, moving forward, turning, and stopping.⁹

To address this issue, Seeman *et al.* constructed a bipedal DNA Brownian motor, illustrated in *Figure 5*, that coordinates the action of its two legs by cyclically catalyzing the hybridization of metastable DNA fuel strands (Seeman *et al.*, 2009).

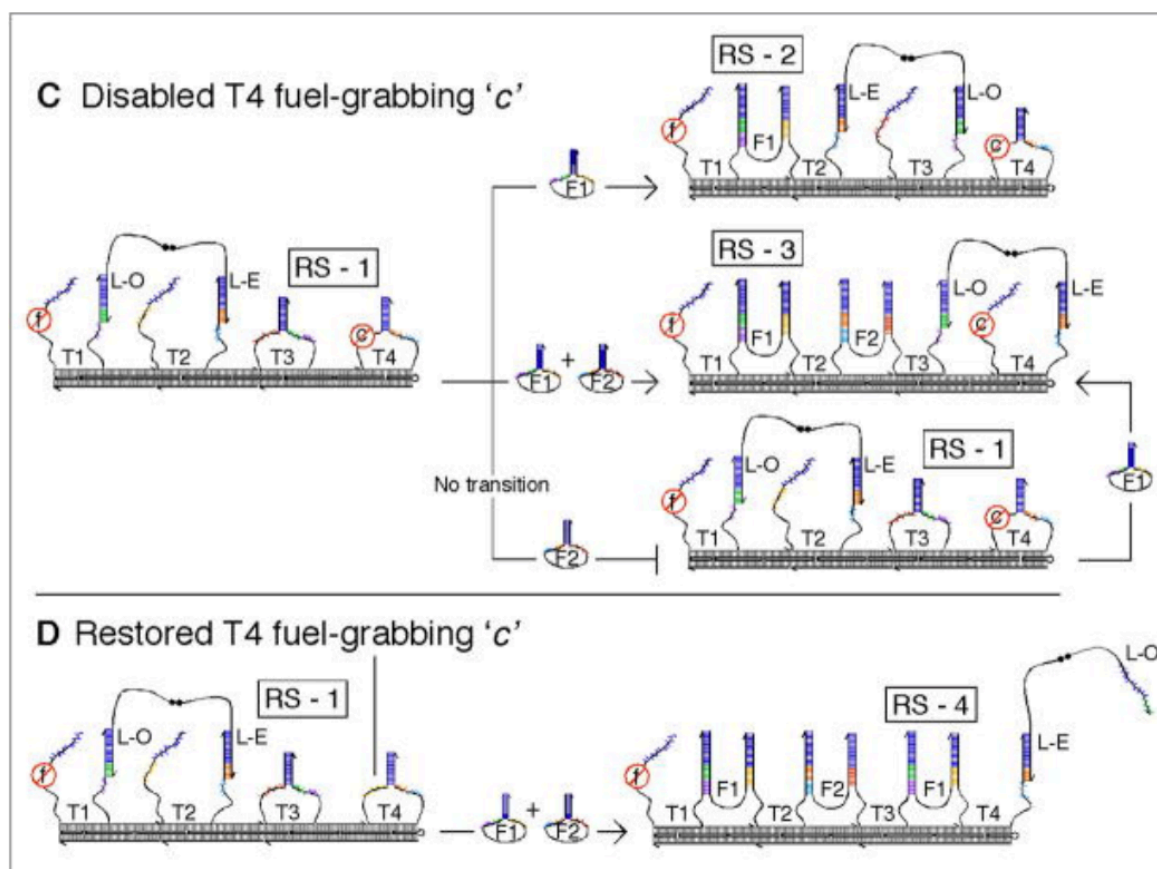


Figure 5. Upon the addition of fuel hairpins F1, the L-O leg of the bipedal walker is kicked off of the stem loop T1 and hybridizes to T3 exhibiting a walking motion from RS-1 to RS-2. When F1 and F2 are added, the walker is able walk further to RS-3. Lastly, when only F2 is added, the walker remains stationary in RS-1. D. After the T4 fuel-grabbing sequence 'c' was restored and an additional F1 hairpin was incorporated, which kicks L-O off of T3, the walker moves further along the track to RS-4.¹⁰

Although the walkers described above are promising, Yehl *et al.* cite that the maximum distance travelled amongst the most processive ones is only 1 μm as these walkers tend to dissociate from the track (Yehl *et al.*, 2016). Additionally, although increasing the number of legs or the multivalency of the motor improves the surface affinity, it consequently reduces speed suggesting a limiting tradeoff of these systems.

To address these drawbacks, Yehl *et al.* designed a far more efficient system, the DNA monowheel (DMW) with the ability to roll over much longer distances, reaching up to 1 mm which is 1000-fold greater than that of the most processive DNA walkers. This molecular motor system involves a rolling rather than a walking motion, which greatly enhances the speed, processivity, and motor efficiency by several orders of magnitude by reducing unproductive sampling interactions with the surface. Via this rolling mechanism, the multivalent nature of a DMW is utilized to maintain high velocity, approaching that of natural motor proteins. This rolling motion involves the binding of free DNA particle strands to new footholds while bound strands are simultaneously cleaved by RNase H, as shown in *Figure 6*. The particle moves in accordance to a burnt bridge mechanism where the free energy of binding new single stranded RNA provides the driving force for movement, biasing Brownian motion away from the consumed substrate (Yehl *et al.*, 2016).

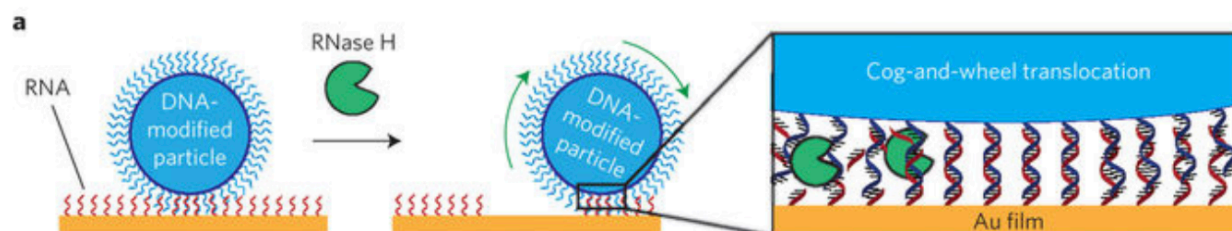


Figure 6. DNA modified particles hybridized to a complimentary RNA monolayer. Particles were immobilized to the surface until RNase H was added, which selectively hydrolyses RNA duplexed to DNA. This hydrolysis caused the particle to detach from the surface at that site allowing it to roll and attach to an adjacent RNA strand.¹³

This design utilized a highly multivalent motor, which moves through a cog-and-wheel mechanism allowing micrometer-sized particles to roll rather than walk. The DNA monowheel (DMW), design by *Yehl et al.*, used in the following experiments is the fastest DNA motor ever built with velocities $\sim 5,000$ -fold greater than that of the fastest synthetic DNA walkers (*Yehl et al.*, 2016). Although the motor reaches high velocities, it also maintains a high level of sensitivity for the detection of the presence of certain molecules as the particle's motion is highly dependent on the molecular interactions the motor makes.

The great processivity of this system can be explained by the high density of DNA and RNA as well as the large contact area between the particle and the surface. These characteristics together decrease the likelihood of the release of the particle from the surface, allowing the particles to travel for long distances of up to 1 mm (*Yehl et al.*, 2016).

Additionally, in other designs, DNAzymes and endonucleases are utilized in place of RNase H. However, *Fang et al.* provides basis for why RNase H is a better choice as the enzyme for a sensitive system. RNase H has a high hydrolysis rate, greater than that for endonucleases and DNAzymes. The turnover number (k_{cat}) of RNase H is $0.95 (\pm 0.10) \text{ s}^{-1}$ which is ~ 100 times faster than that for exonuclease III surface hydrolysis of double stranded DNA microarrays and therefore RNase H powered motors can achieve faster velocities (*Fang et al.*, 2005). *Yehl et al.*

also found its turnover rate to be 6,000-fold greater than that for nanoparticle-immobilized DNAzymes for an optimally passivated surface (Yehl *et al.*, 2016)

Additionally, a truly noteworthy discovery, which illuminates the possibilities of this system, is in its ability to detect single-nucleotide polymorphism (SNP). The monowheel rolling motion is highly sensitive to the kinetics of RNase H-catalyzed RNA degradation and, therefore, could obtain sensing on the molecular level. Yehl *et al.* tested the system's ability in detecting a SNP mutation. It was found that particles with the SNP travelled ~60% slower than particles without the SNP as shown in *Figure 7*. This graph suggests that the mean displacement of the perfect match particles, 15 minutes after the addition of RNase H, was significantly higher than that for the particles with the SNP ($P < 0.0001$). The difference in velocity could be attributed to a slower rate of hydrolysis for RNase H to hydrolyze duplexes with this SNP. With only a single nucleotide difference, this significant reduction in velocity suggests the highly sensitive and useful nature of this motor. Importantly, SNP sensing was performed using a low-cost cellphone camera microscope, demonstrating the unique capability to use brightfield imaging for highly-sensitive molecular detection (Yehl *et al.*, 2016).

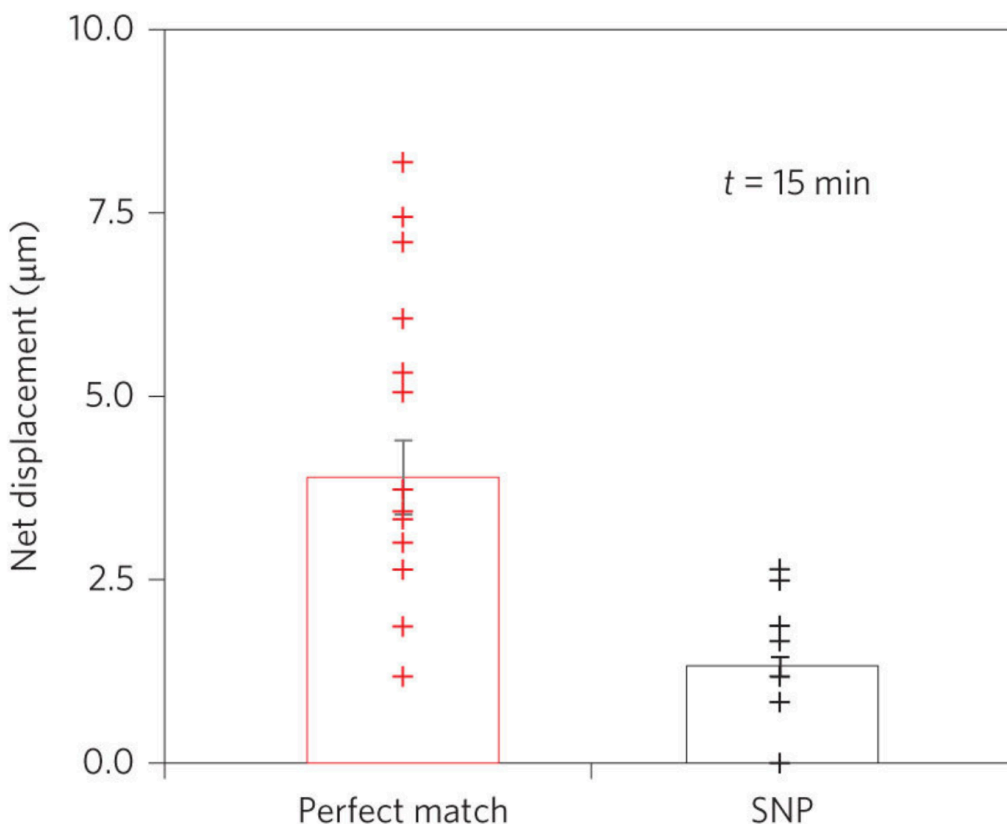


Figure 7. Scatter plot showing the net displacement (μm) of the particles 15 minutes after the addition of RNase H. The heights of the bars represent the mean displacements. The error bars on the bar graph represent the standard deviation with $n = 42$ particles total giving a $P < 0.0001$, as determined by a t -test with unequal variance.¹³

Because it has previously been shown that the velocity of the particles can be modulated by molecular interactions between the particle and the planar substrate, it was next sought to determine whether the particles could be used to sense soluble biomolecules. Such capabilities could ultimately lead to useful applications such as disease diagnosis. Indeed, previous work has shown that the speed of the DNA particle can be modulated by the presence of target oligonucleotides. This is possible by engineering the particles such that target

oligonucleotides would bind the particle to the surface through Watson-Crick base pairing and prevent further motion, acting as “molecular locks”. However, oligonucleotides only constitute a small subset of biomolecules. DNA monowheels would provide a molecular sensing utility if they could be used to sense proteins as well as oligonucleotides.

In the following experiments, biotin was doped on both the particle and the surface to detect streptavidin. This design attempts to further apply this system in detecting specific molecules and uses the well-documented, high affinity biotin-streptavidin interaction to study the sensitivity of the system. Therefore, the overarching research question of the following experiments is “Can DNA monowheels be used to detect proteins using brightfield microscopy?” To answer this question, the experimental design utilizes the multivalent characteristic of streptavidin as well as the high binding affinity of the noncovalent interaction between biotin and streptavidin. This strong interaction creates a distinct halt in the DNA monowheel system and, thereby, reduces the speed of a particle rolling on a biotinylated surface. This bond cannot be cleaved by RNase H, distinguishing it from particle DNA and surface RNA chimera interactions.

This high affinity and its origins were investigated by Weber *et al.*, stating that the dissociation constant (K_d) of the binding of biotin to streptavidin is 10^{-15} M. Factors which contribute to this strong interaction include the formation of multiple hydrogen bonds and van der Waals interactions. Structural alterations can be made at the biotin binding site to induce quaternary changes in streptavidin and further strengthen the interaction (Weber *et al.*, 1989).

As depicted in *Figure 8*, the motor consisted of a DNA-coated spherical particle, with a diameter of 5 μm , which hybridized to a gold surface modified with complementary RNA

strands. Each particle had a density of $\sim 91,000$ molecules μm^{-2} , which complemented the RNA density on the surface to optimize the degree of polyvalency of the rolling and minimize particle detachment at $\sim 10^{2-3}$ contacts/ μm^2 .

Initially, the surface was functionalized with different ratios of DNA anchor strands and biotinylated DNA anchor strands. Then, SH-PEG (thiolated polyethylene glycol) was added to passivate the surface in order to prevent RNase H from non-specific sticking to the gold surface that would inactivate the RNase H. Additionally, this step prevents any non-specific binding of the particle, biotin or streptavidin to the surface. This sticking could slow the system and, therefore, skew the results creating a sub optimal tracking system. RNA was added to form RNA/DNA chimeras tagged with Cy3 to allow for later quantification of RNA density on the surface. A surface with a lower than ideal RNA density was analyzed with caution and the experiment was duplicated.

Then, particles were functionalized with biotinylated DNA and incubated with varying concentrations of streptavidin or no streptavidin for conventional particles used in control wells. Upon addition of RNase H, which selectively hydrolyses hybridized RNA, the particle was freed from the surface at that site allowing it to roll. However, at such sites where streptavidin is bound to biotin on the surface and particle, the particle remained stationary as the RNase H couldn't destroy this bond as shown in *Figure 8*.

Table 1 shows the sequences for the oligonucleotides used in the experiments with the structures of each of the abbreviated RNA and DNA modifications. These sequences show the complementarity between the DNA anchor and the DNA portion of the RNA/DNA chimera as well as the complementarity between the particle DNA and particle biotin strand with the RNA

portion of the RNA/DNA chimera. This complementarity is the foundation for the mechanisms described earlier which allow the particle to bind to the surface. The bases underlined in *Table 1* are sites where RNase H cleaves off RNA, thereby freeing the particle. The streptavidin, however, is added to put a wrench in this system, slowing the particle and thereby counteracting the action of RNase H, as shown in *Figure 8*.

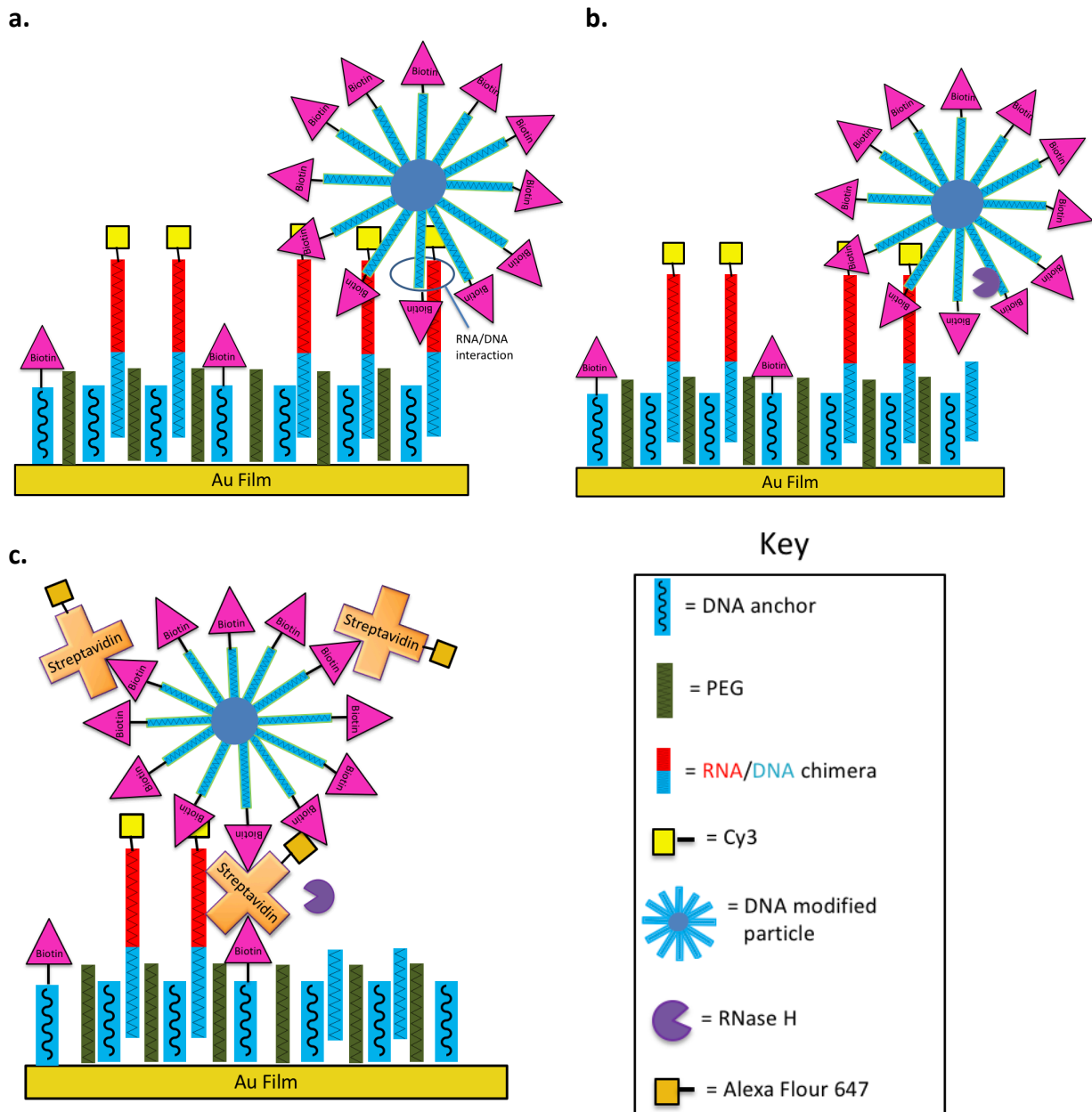


*Figure 8: Scheme of the halting of 100% biotinylated particles rolling atop a gold surface coated with a certain concentration of biotin. **a.** Complimentary particle DNA strand hybridizes to its complimentary RNA strand of the DNA/RNA chimera bound to the surface thereby holding the particle to the surface. **b.** RNase H cleaves this RNA/DNA interaction thereby freeing the particle and allowing it to roll and form another interaction at a neighboring RNA strand. **c.** In the presence of streptavidin, the biotin on the surface and particle bind halting the particle. This interaction cannot be broken by RNase H. in the presence of streptavidin biotin on the particle (Note: this figure is not drawn to scale).*

Table 1: Modified oligonucleotide sequences

Name	Sequence (5' – 3')
Particle Biotin	/5Hexynyl/TTTTTTTTTTTTTTAGTAATCAATCACAG/3Bio/
Strand	
Particle DNA	/5Hexynyl/TTTTTTTTTTTTTTAGTAATCAATCACAG
DNA Anchor	/5AmMC6/GAGAGAGATGGGTGCTTTTTTTTTTTTTTT/3ThiolMC3-D/
RNA/DNA Chimera	GCACCCATCTCTCTCrCrCrCrCrCrCrUrGrArUrUrGrArUrUrArCrU/3Cy3Sp/
Substrate	

Surface Biotin /5Bio/TTTTTTTTTTTTTTTTTTTTTTTTTTTTTTTTTTTT/3ThiolMC3-D/

Strand

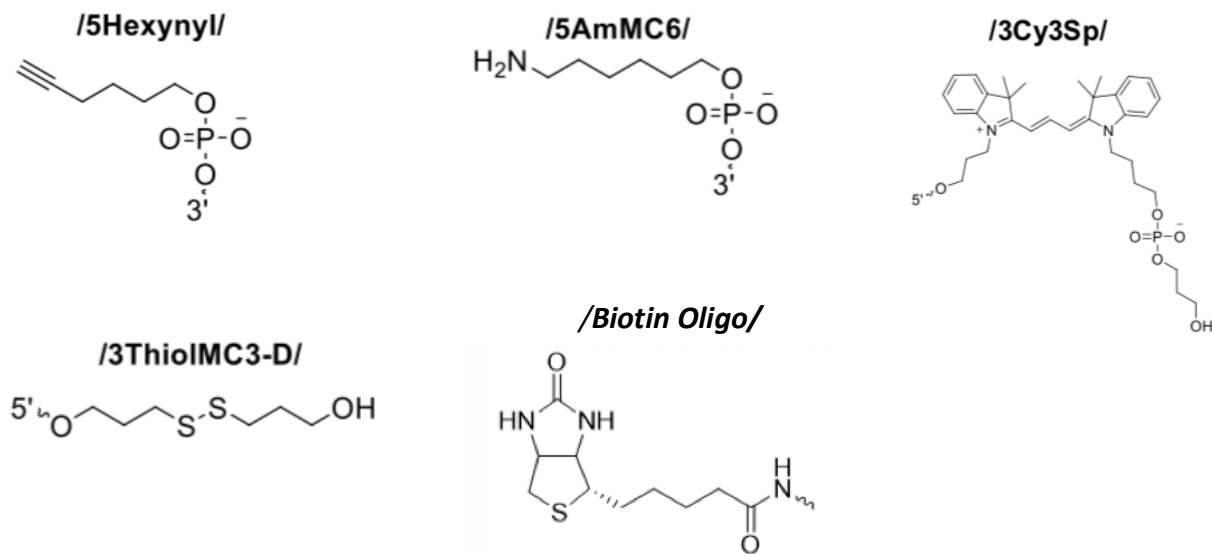


Table 1. Table with the sequences of the oligonucleotides used with the bases that represent RNase H recognition sites underlined. Directly below the table, are illustrations of the DNA and RNA modifications.^{2, 13}

2. Experimental Methods

The experimental methods were adapted from Yehl *et al.*'s work. These procedures include the method for thermal evaporation of gold onto a glass slide, the fabrication of RNA monolayers as well as the synthesis of azide functionalized particles and high-density DNA particles. Additionally, the imaging procedures from this paper were followed to measure the RNA intensity and the velocities of the particles as well as to acquire images of depletion tracks (Yehl *et al.*, 2016).

2.1. Thermal evaporation of gold films

Two 25 mm x 75 mm were cleaned by sonication in DI water for 5 minutes and then again in fresh DI water for 5 minutes. Next, the slide was sonicated in ethanol for 5 minutes and then dried under a stream of N₂. The cleaned slide was then placed inside a thermal evaporator chamber located in the Emory University Math and Science building. First, the chamber's pressure was reduced to 50×10^{-3} Torr and then flushed three times with N₂. The pressure was further reduced to $1-2 \times 10^{-7}$ Torr using the turbo pump and liquid N₂ to cool the chamber. Next, chromium was evaporated onto the slide at a rate of 0.2 Å/sec until it reached a thickness of 20 Å. Chromium acted as the adhesive allowing gold to bind to the surface. Lastly, gold was evaporated onto the surface at a rate of 0.4 Å/sec until it reached a thickness of 100 Å.

2.2. Implementation of wells with IBIDI flow chambers

An IBIDI stick-Slide VI^{0.4} flow chamber, containing six channels (17 x 3.8 x 0.4 mm dimensions), was adhered to the Au-coated slide. Each channel was then flushed with ~5 ml of DI water.

2.3. Fabrication of DNA and biotinylated anchors of varying proportions

SH-DNA with amine and biotinylated DNA (T30B) were both diluted to a concentration of 1 μM in 1 M Potassium Phosphate buffer. These strands served as the anchor to which the DNA portion of the RNA/DNA chimeras added later on, was hybridized. SH-DNA was used as thiol groups bind to the gold on the surface. For 100% DNA (conventional) wells, 40 μL of 1 μM SH-DNA with amine was added to each well whereas for the 25% biotin wells, the 1 μM SH-DNA and T30B were added in a 1:3 ratio. For the other percentage biotin wells, the ratio was tuned for their respective proportions. Each chamber was then sealed with Parafilm and placed inside a petri dish along with an opened Eppendorf tube of ~200 μL water to prevent evaporation. The petri dish was also sealed with Parafilm as further precaution as the DNA and biotin anchors were left to incubate in the wells overnight.

2.4. Passivation of the surface

Next, the wells were each washed with ~5 mL of DI water to remove any excess, unbound DNA and biotin. The surface of each well was then passivated with 40 μL of 100 μM of $\text{SH}(\text{CH}_2)_{11}(\text{OCH}_2\text{CH}_2)_6\text{OCH}_3$ (SH-PEG) solution diluted from stock in 5 parts DI water, 4 parts ethanol. SH-PEG was added to block any bare spots on the gold surface where streptavidin

might non-specifically bind as well as to maximize the hybridization of RNA to the DNA anchoring strand. The wells were left to incubate for 6 hours, using the evaporation safeguards described above, however, this time with an opened Eppendorf tube containing the ethanol, water mixture.

2.5. Hybridization of RNA to DNA anchoring strands

Each well was then washed with ~5 mL of ethanol then ~5 mL water to remove excess, unbound SH-PEG. Next, the RNA/DNA chimera was added to the surface with the DNA portion of the chimera hybridizing to the DNA anchors. Then after at least 12 hours or upon imaging, the wells were washed of excess RNA each with 5 ml of 1x PBS. Lastly, the RNA substrate was immobilized to the surface through hybridization of 100 μ l of a complementary RNA/DNA chimera (100 nM) in 1 \times PBS for 12 hours. The wells were sealed with Parafilm for each step to prevent evaporation and the resulting RNA monolayer remained stable for weeks, as determined by fluorescence imaging.

2.6. Synthesis of azide functionalized particles

First, 1 mg of 5- μ m animated silica beads was mixed with 1 mg of N-hydroxysuccinimide azide heterobifunctional linker. This mixture was then diluted in 100 μ L DMSO and 1 μ L of a 10x diluted TEA (trimethylamine) stock in DMSO. The reaction proceeded overnight, and the azide-modified particles were purified by adding 1 ml of DI water and centrifuging down the particles at 15,000 revolutions per minute (r.p.m.) for five minutes.

Then, the supernatant was discarded and resuspended in 1 mL DI water. This procedure was repeated 7 times except after the last centrifugation, ~0.7 mL was discarded leaving about 30 μ L of a concentrated particle stock. The azide-modified particles were then kept in the cold room (4 °C).

2.7. Production of high density DNA silica particles

To make high density DNA functionalized silica particles, 5 μ L of 1mM alkyne modified DNA were added to 5 μ L of the azide-functionalized particles. Next, this mixture was diluted with 25 μ L of DMSO and 5 μ L of 2M TEAA (triethyl ammonium acetate) buffer. Then, 4 μ L of water saturated with L-ascorbic acid was added to the mixture. Lastly, 5 μ L of the copper catalyst aliquot, made from 10 mM Cu-TBTA (Tris[(1-benzyl-1*H*-1,2,3-triazol-4-yl)methyl]amine) in 55 vol % DMSO, was added to initiate the cycloaddition of the alkyne modified DNA to the azide-functionalized particles. The reaction vessel was left to incubate for at least 2 hours in the lab bench.

Then, the DNA silica particles were washed first with 1 mL of a solution of 10% of a 10% Triton-X solution and 90% 1x PBS and then centrifuged for 5 minutes at 15,000 rpm for five minutes. Then the supernatant was carefully discarded, and the particles were gently resuspended in the Triton-X solution. This solution was then centrifuged in the small centrifuge on the lab bench for about 1 minute. Next, the supernatant was again carefully discarded except this time the particles were resuspended in 1x PBS and placed in the small centrifuge for 1 minute. This process was repeated 2 more times for a total of 3 washes in PBS. Following the last wash, the supernatant was discarded to achieve a final volume of ~50

μL , and the particles were placed in the cold room to be stored with minimal light exposure until use.

2.8. Synthesis of biotinylated silica particles

To make 100% biotinylated silica particles the above procedure for DNA silica particles was repeated except with 5 μL of 1 mM particle biotin strand. To make 1% biotinylated silica particles, used in earlier experiments, 5 μL of 1 mM alkyne modified DNA and 1 μL of 0.05 mM particle biotin strand diluted in DI water was added.

2.9. Addition of varying concentrations of streptavidin to biotinylated particles

Varying concentrations of streptavidin could be incubated and therefore bound to the biotin on the 100% biotinylated particles. First, varying concentrations of 100 μL of streptavidin in 1x PBS were made in separate Eppendorf tubes. Commonly used concentrations include 0 nM (just PBS), 0.03 nM, 0.3 nM, 1 nM and 100 nM to provide a large array of concentrations with smaller increments between concentrations in the range which yielded a 50% decrease in speed in previous experiments. Then, 2 μL of 100% biotinylated particles were added to each of the tubes and stored in the cold room overnight to allow the streptavidin time to bind to the particles.

After incubation, the particles were washed 3 times with 1x PBS, the first time for 5 minutes at 15,000 rpm and the next two times in a small benchtop centrifuge for 1 minute each time. After the last wash, an extra 80 μL of supernatant was disposed to leave 20 μL of a more concentrated solution of particles such that a satisfactory number of particles could

be viewed within each viewing frame during imaging. Additionally, these washes were imperative for getting rid of any excess streptavidin and thereby preventing unbound streptavidin from binding to the surface biotin upon addition of the particles to the surface.

Note: In earlier experiments the streptavidin was incubated and left to bind to the biotin on the surface rather than on the particle. However, in more recent experiments, the assay was essentially the same but flipped such that the streptavidin was bound to 100% biotinylated particles. This change in experimental design was made to ensure streptavidin had sufficient time to bind to the biotin. With the particles, it was easier and less time consuming to leave overnight to allow streptavidin to fully bind. With the old design, the surface wasn't usable during the time it was left to incubate with streptavidin, which would stall the progression of the experiment by the two hours left to allow for streptavidin binding. Additionally, the particles could be more adequately washed than the surface. Completing five washes with 1x PBS by centrifugation ensured the vast majority, if not all, of the streptavidin was, in fact, bound to the biotin on the particle and not just free in solution.

2.10. Preparation of rolling solution & imaging

To make the rolling solution, 100 μL of formamide, 50 μL of 10x RNase H reaction buffer (25 mM Tris pH 8.0, 8 mM NaCl, 37.5 mM KCl, 1.5 mM MgCl_2), 75 μL of 10% Triton and 775 μL DI water were added to an Eppendorf tube. For each experiment, this procedure was duplicated to allow for enough rolling solution for 12 wells. Next, 23 μL of 500 μM DTT in PBS was added to a tube with 1 μL RNase H and immediately placed in an ice box. Then, 180 μL of this rolling solution was added to each aliquot of particles and 40 μL of this solution was

added to each well in accordance with their streptavidin concentration assignments, vortexing immediately prior to each addition.

Then, at least 20 regions of interest (ROIs) were found for each well using the brightfield setting on the Nikon Eclipse Ti TIRF microscope at 20x magnification. Next, an additional 40 μL of a solution containing 150 μL rolling solution and 6 μL of the RNaseH/ DTT was carefully added to each of the three wells without touching the edges of the wells to avoid alteration of the previously programmed ROIs. This RNase H solution was used to initiate the RNA hydrolysis reaction as RNase H cleaves RNA, thereby freeing the particle and allowing it to roll.

The brightfield imaging time was then set to ~ 20 minutes at 2-minute intervals using Nikon Elements Software and time lapses of each of the wells at each ROI were acquired. Lastly, high-resolution epifluorescence images (100x) of fluorescence depletion tracks were taken to ensure that particle motion was due to continuous RNase H hydrolysis rather than just Brownian motion. The tracks showed a darker color as the RNase H had cleaved the Cy3 fluorescently tagged RNA chimera at these places.

2.11. Particle Trajectory Analysis

To quantify the velocities of the particles, a custom-written MATLAB code was used to track particle movement and the mean displacement was taken at 20 minutes for each particle and averaged for each well with differing concentrations of streptavidin. These were then plotted against the log of streptavidin concentration. Additionally, a fit line was made for the data set to find the midpoint at which the particles slowed to half the optimal speed.

Additionally, in some experiments, the mean squared displacement was plotted against time-lag to determine the MSD scaling exponent (α), whose implications are described in the following section.

2.12. Streptavidin Fluorescence Calibration

To determine the streptavidin concentrations to be used in the experiments, the streptavidin fluorescence was calibrated to find the concentration at which the biotinylated surface is saturated, which would serve as the maximum concentration. Then, the concentrations from 0 nM to the concentration of total saturation on a log scale could be used for the experiments. To do this, 0, 10, 25 and 50 nM of streptavidin were incubated on 0.1 and 0.01% biotin surfaces and the Alexa 647 fluorescence was measured in 1 second intervals and 5% laser power on the microscope.

2.13. Testing for non-specific binding of streptavidin using flow cytometry

To test for non-specific binding of streptavidin to the particle, flow was used to measure the fluorescence of particles incubated with Alexa 647 tagged streptavidin then washed with PBS. In the absence of biotin, streptavidin should not stick to the particle unless non-specific binding has occurred and therefore, if there is Alexa 647 intensity when the particles were run through flow, there was at least some non-specific binding. This was done for particles incubated for two hours in 0.1 nM, 1 nM and 10 nM streptavidin.

3. Results and Discussion

First, non-specific binding of streptavidin to the particle had to be tested using flow cytometry. *Figure 9a* shows the absence of significant non-specific binding for particles incubated overnight with 0.1 nM and 1 nM streptavidin concentrations. However, at 10 nM there seemed to be some non-specific binding and therefore it was difficult to make the same conclusions. Therefore, positive controls of 100% biotin particles incubated with 0, 0.01, 0.03, 0.1, 0.3, 1, 10, 100 nM streptavidin were measured, which yielded much greater intensities as high as 36,293 for 100 nM streptavidin.

The fluorescence intensities of 100% and 0% biotin particles incubated with 10 nM streptavidin were compared in *Figure 9c*. The 0% biotin particles had a fluorescence intensity of 3374, while the 100% biotin particles had an intensity of 36293, over 10-fold greater, shown in *Table 2*. Additionally, the histogram of intensity shows no overlap in particle intensity measurements between the two and a z-test confirmed that the difference in fluorescence is, in fact, statistically significant ($p < 0.01$). Therefore, non-specific binding of streptavidin to the 0% biotin particles isn't significant at nanomolar concentrations and the DMW model can be used in biotin-streptavidin detection.

Testing non-specific and specific binding of streptavidin to the particle using flow cytometry

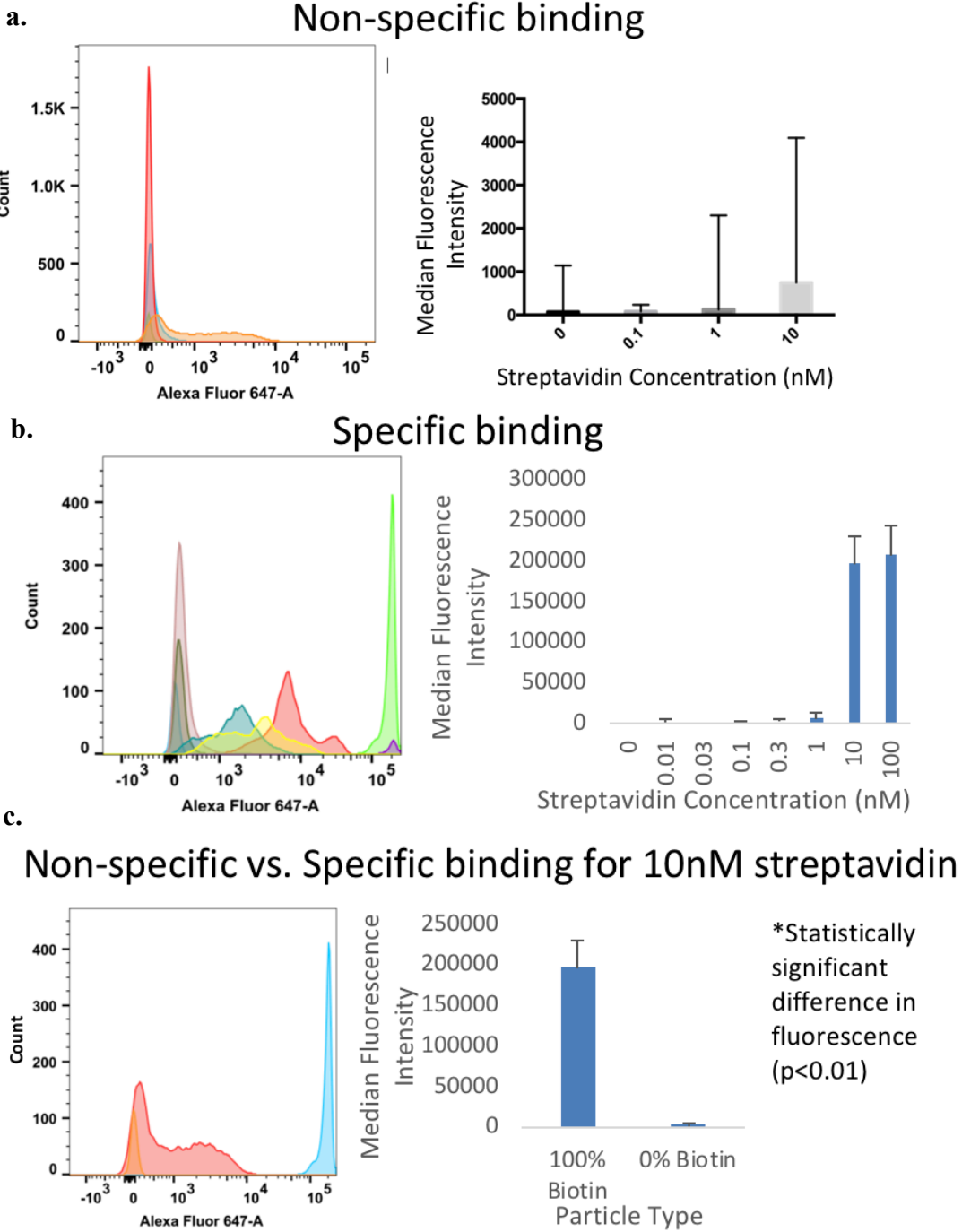


Figure 9. Concentration dependence of streptavidin non-specific binding on the particle using flow cytometry. **a.** Alexa 647 fluorescence measurements of 100% DNA particles incubated overnight with 0, 0.1, 1, 10 nM streptavidin. **b.** Fluorescence measurements

for 100% biotinylated particles incubated with 0, 0.01, 0.03, 0.1, 0.3, 1, 10, 100 nM streptavidin indicating full saturation at about 10 nM streptavidin. **c.** Comparison of 100% and 0% biotin particles incubated with 10 nM streptavidin suggesting that there is minimal non-specific binding to the 0% biotin particles by the large difference in streptavidin intensity ($p < 0.01$).

Table 2: Alexa 647 Fluorescence Measurements using flow cytometry

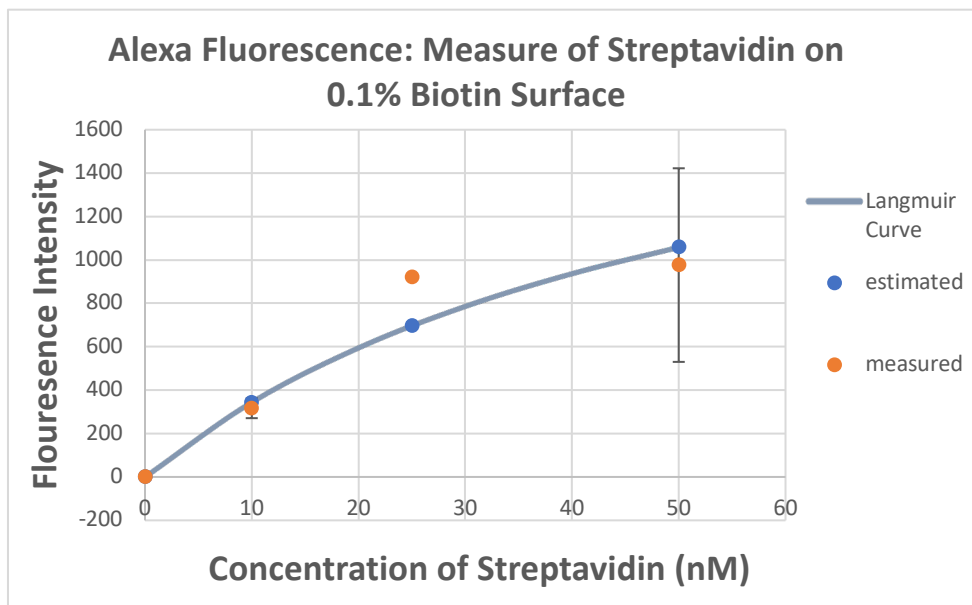
Streptavidin concentration (nM)	# of particles	Median Alex Fluor 647 Intensity	Standard Deviation of Alexa Fluor 647 Intensity
DNA Particle (non-specific binding test)			
0	1002	71.9	1072
0.1	10000	80.9	154
1	6041	127	2177
10	8038	747	3374
100% Biotin Particles (specific binding test)			
0	942	100	60.6
0.01	1955	182	5060
0.03	4344	212	298
0.1	3402	1585	1172
0.3	3414	2793	3391
1	4321	6718	8372

10	3271	196430	34902
100	212	206876	36293

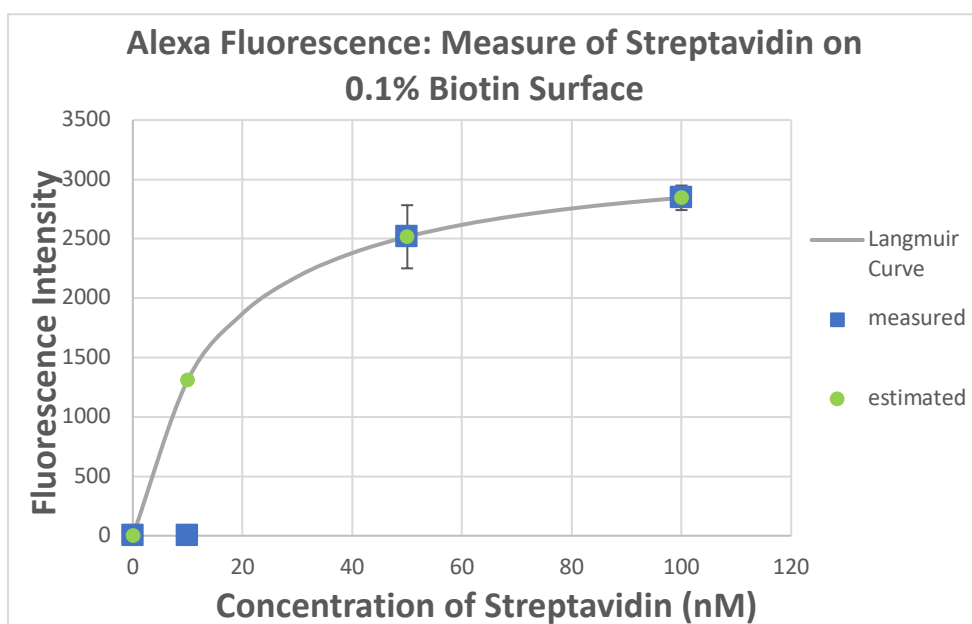
Then, as another preliminary experiment, a calibration curve was calculated for streptavidin by solely measuring the Alexa 647 concentrations at each of the streptavidin concentrations on 0.1% and 0.01% biotin surfaces as shown in *Figure 10*. These intensities were measured using 1 second exposure time and 5% laser power on the TIRF microscope. The Langmuir binding equation, $I = I_{\max} * c / (c_{50} + c)$ where I is the Alexa 647 fluorescence intensity, c is the streptavidin concentration, I_{\max} is the maximum intensity and c_{50} is the streptavidin concentration yielding 50% of maximum intensity. This equation was used to find the estimated intensities at each streptavidin concentration as well as c_{50} . The calibration for the 0.1% biotinylated surfaced gave a c_{50} of 53.9 nM had to be repeated as the fluorescence intensity was drastically lower for 100 nM than that for 10 nM streptavidin, 330.2 and 976.3 respectively. This data point was excluded from the graph as to not skew the entire fit. Then, once repeated, the c_{50} was found to be 14.9 nM.

Given the c_{50} values of 14.9 and 53.9 nM and the tapering of the measured values in the range of 25-50 nM, it was concluded that at ~100 nM the surfaces would be almost or entirely saturated. These findings provided basis for future experimental designs using a streptavidin concentration range of 0 to 100 nM. For experiments using surfaces with percentages of biotin other than 0.1%, this range was still found to be effective, evident through the particles' velocity measurements.

a.



b.



c.

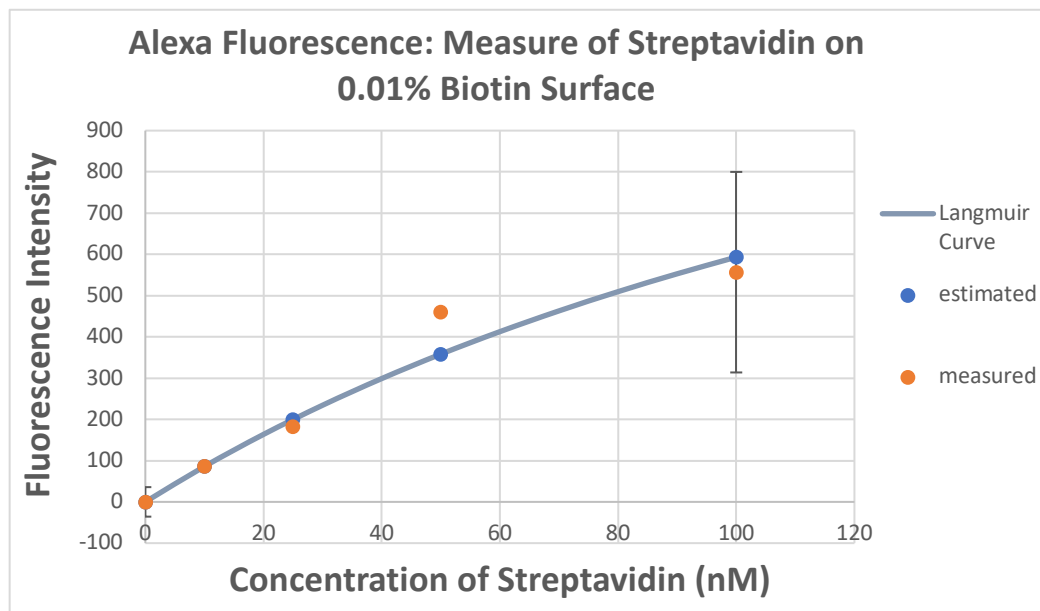
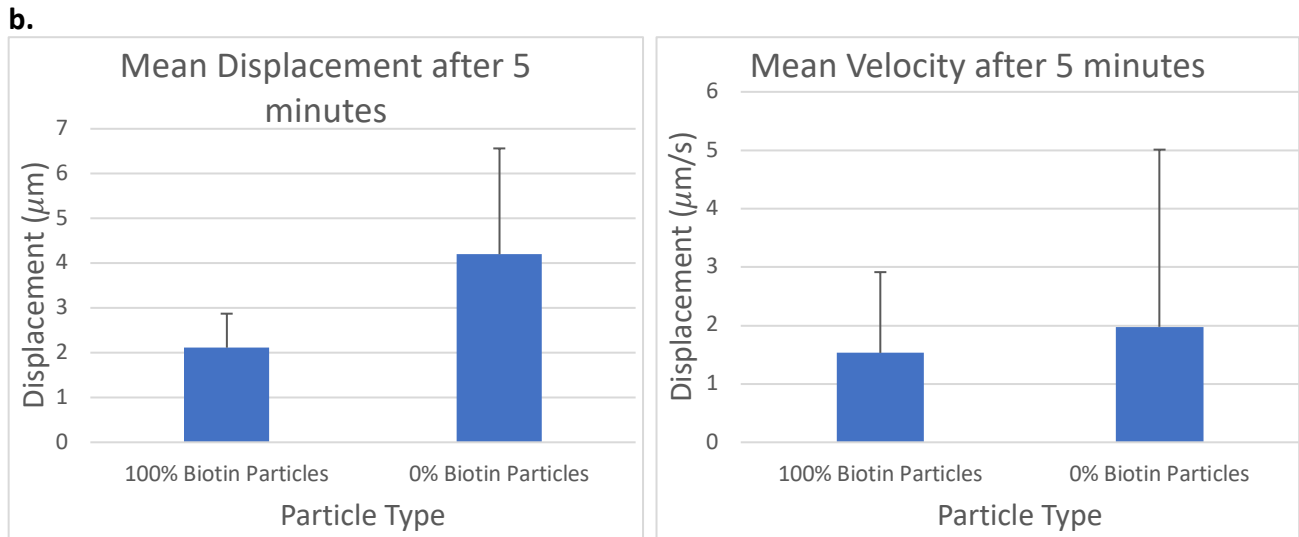
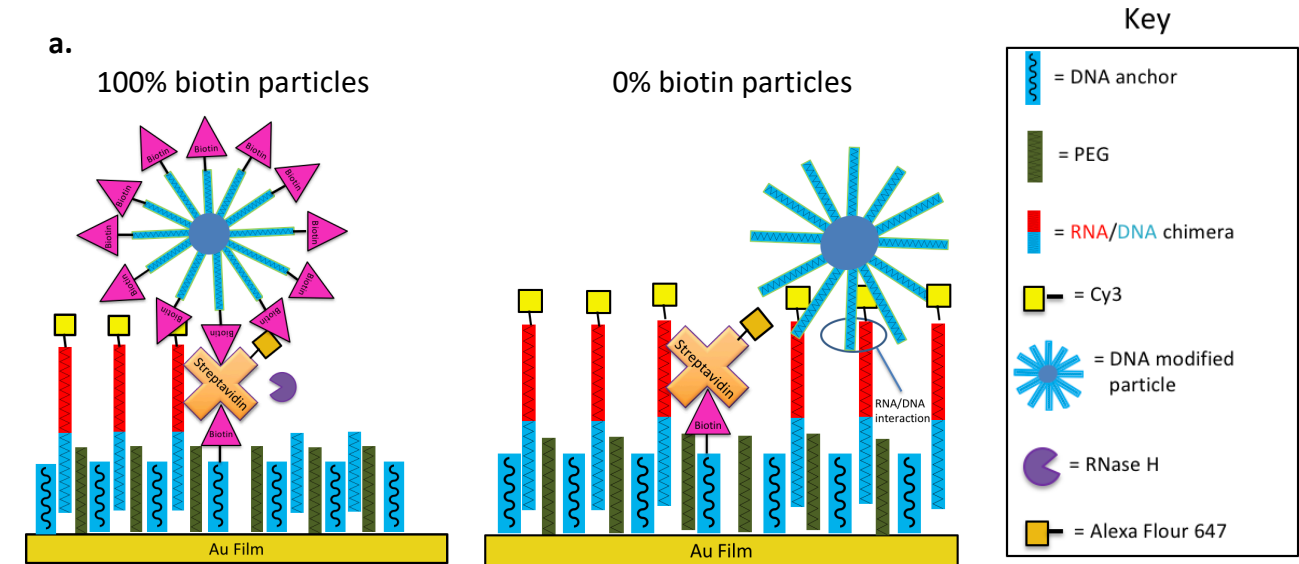


Figure 10. Langmuir curve for the binding of streptavidin to 0.1% biotinylated surfaces at a 5% laser power, 1 second exposure time and 3 fluorescence intensity measurements per streptavidin concentration. **a.** Measure of streptavidin fluorescence on a 0.01% biotinylated surface giving a c_{50} of 53.9 nM. This calibration had to be repeated as the fluorescence intensity drastically decreased to 330.2 at a streptavidin concentration of 100 nM. **b.** Repeated calibration experiment for a 0.1% biotinylated surface giving c_{50} =14.9 nM. **c.** Calibration experiment for streptavidin on a 0.01% biotin surface giving c_{50} =191.1 nM.

Next, as shown in Figure 11, the speed of 100% and 1% biotin particles as well as regular (100% DNA, 0% biotin) particles were measured on 1% biotin surfaces incubated with 100 nM of streptavidin. Therefore, the only variable, which was changed was the percent biotin on the particle.

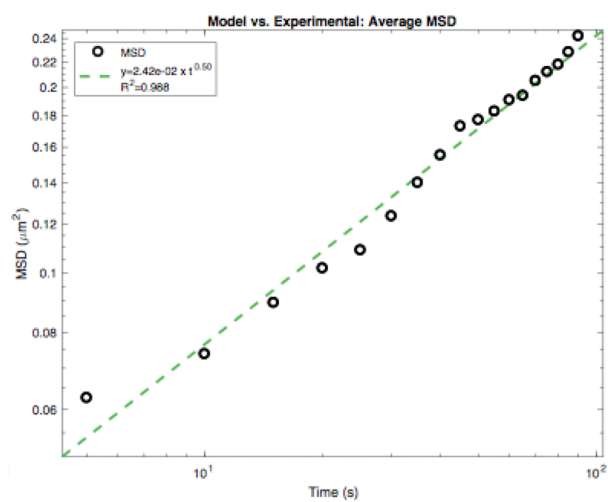
100% and 0% biotin particles on a 1% biotin surface with 100 nM streptavidin incubated on the surface



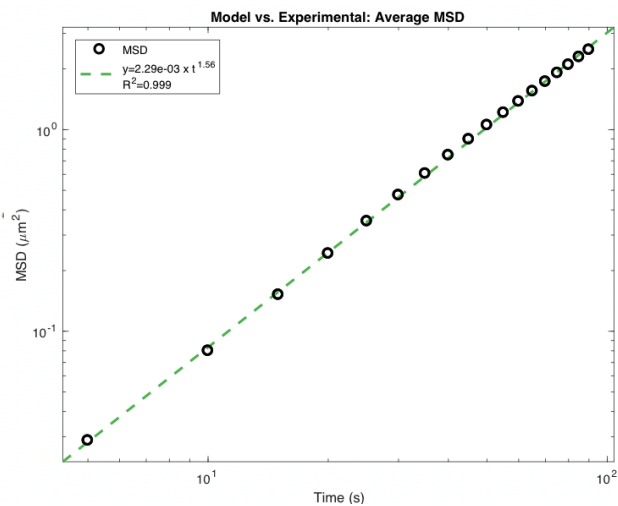
c.

	Final Displacement (µm)		Velocity (µm/s)	
	Mean	Standard Deviation	Mean	Standard Deviation
100% Biotin Particles	2.11	0.759	1.53	1.38
0% Biotin Particles	4.20	2.36	1.98	3.03

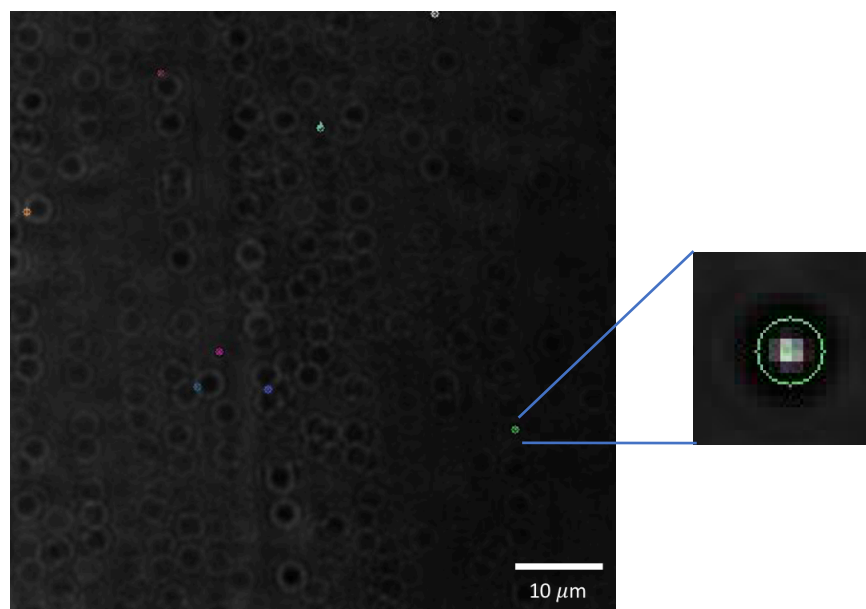
d. 100% Biotin Particles



0 % Biotin Particles



e. 100% Biotin Particles



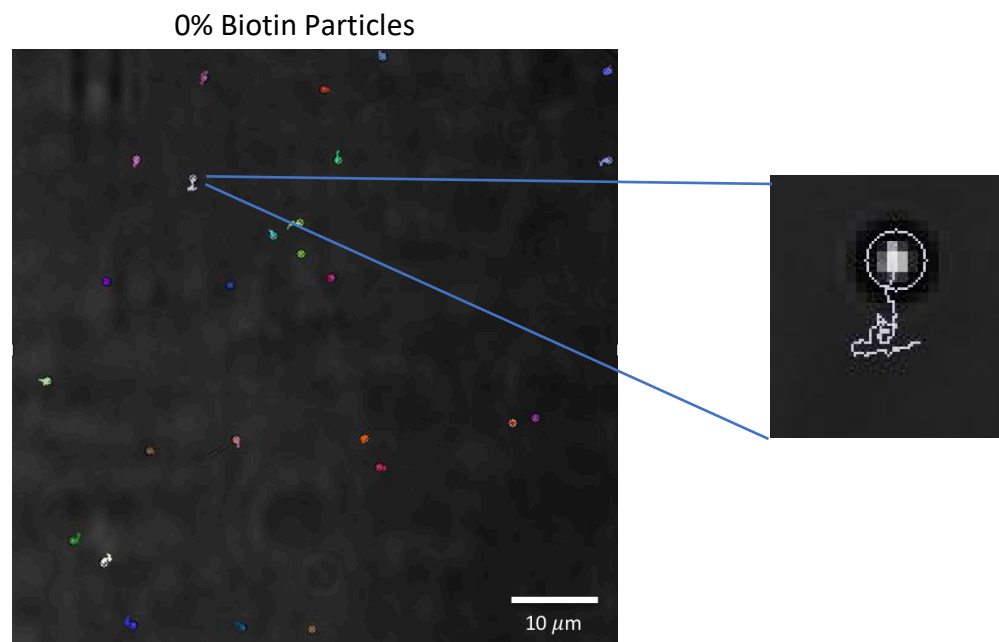
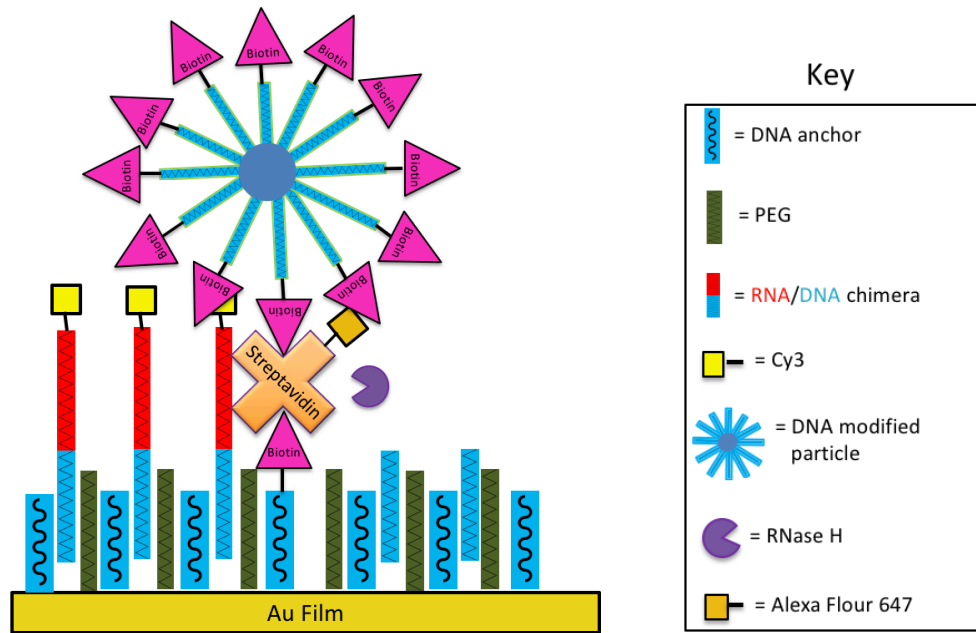


Figure 11. Measure of the velocities and mean squared displacements of 0% and 100% biotin particles on a 1% biotin surface incubated with 100 nM streptavidin for two hours. **a.** Schemes for each experimental design. **b.** MSD (mean squared displacement) plotted against time to give $\alpha=0.5$ for 100% biotin particles and $\alpha=1.56$ for 0% biotin particles. Additionally velocity is plotted against the number of occurrences showing a peak at a lower velocity for the 100% biotin than the 0%. **c.** The mean final displacement and velocity both are significantly lower for the 100% biotin particles than for the 0% biotin particles. Standard deviations are also given for each value. **d.** MSD (mean squared displacement) plotted against time to give $\alpha=0.5$ for 100% biotin particles and $\alpha=1.56$ for 0% biotin particles. **e.** The trajectories with a zoom in at one particle's trajectory for each experimental design giving visible, qualitative evidence to the difference in velocities.

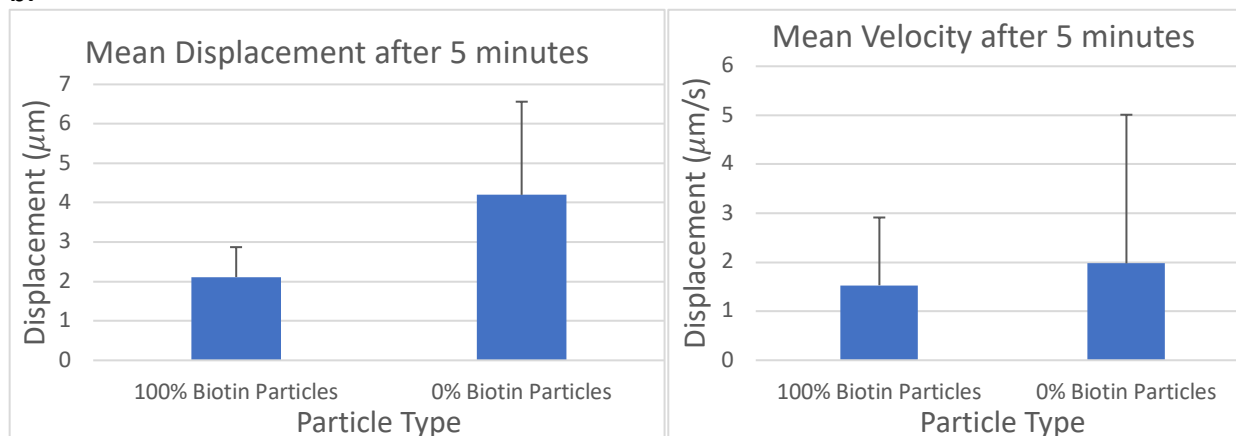
Then, instead of varying the percent biotin on the particle, the percent of biotin on the surface was varied with 1%, 0.1% and 0.01% biotin using only 100% biotin particles and, again, 100 nM streptavidin for each surface as shown in *Figure 12*.

100% biotinylated particles on 1% and 0.1% biotin surfaces incubated with 100 nM streptavidin

a.



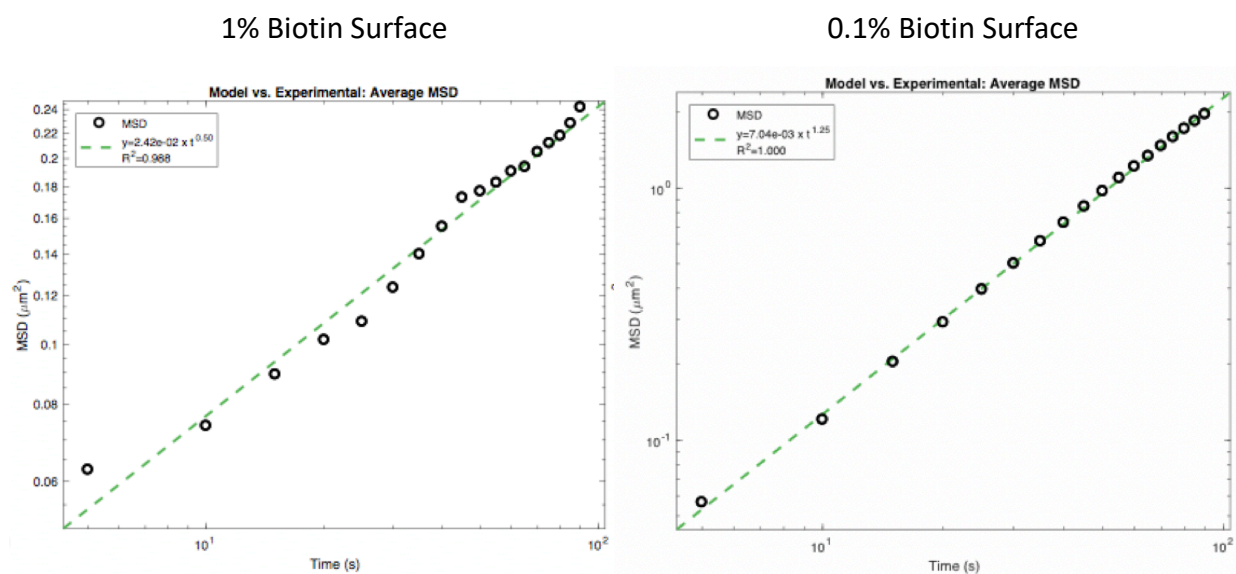
b.



c.

	Final Displacement (μm)		Velocity ($\mu\text{m/s}$)	
	Mean	Standard Deviation	Mean	Standard Deviation
1% Biotin Surface	2.11	0.759	1.53	1.38
0.1% Biotin Surface	3.93	2.31	1.98	1.31

d.



e.

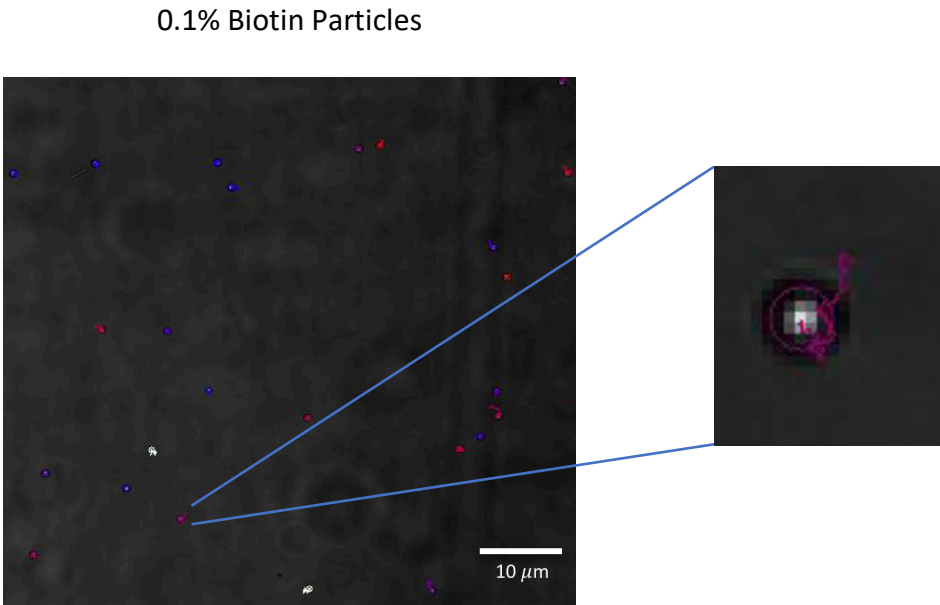
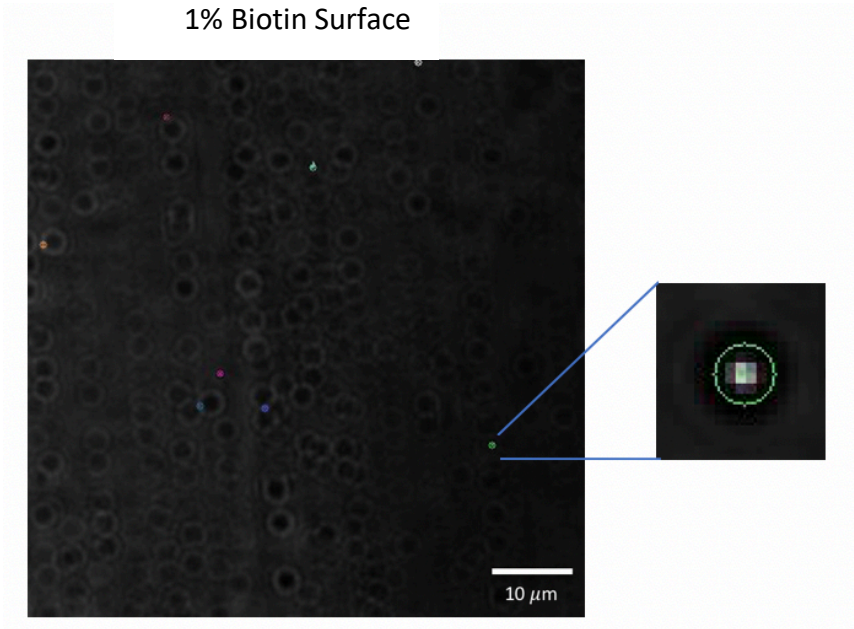


Figure 12. Varying the percentage biotin on a surface incubated with 100 nM streptavidin for two hours using 100% biotinylated particles. **a.** Scheme for the experimental design (note: difficult to depict due to simplicity of the scheme, however, the concentration of biotin on the surface is 10X lower for the 0.1% biotin surface in comparison to the 1% surface). **b.** MSD (mean

quared displacement) plotted against time for 0% and 1% biotin articles. Additional plots show the peak at slightly lower velocity for the 1% biotin surface and displacement and velocity both for the 0% and 1% biotin surface. Standard deviations are shown for $\alpha=0.5$ for 1% biotin surface and $\alpha=1.25$ for 0% biotin surface. *a. Mean squared displacement for one particle's trajectory for each surface. b. Mean squared displacement for 100 particles for each surface. c. The mean squared displacement and velocity both for the 0% and 1% biotin surface. d. MSD plotted against time to give a linear relationship for 100 particles. e. The trajectories with a zoomed-in view of the first 100 ms giving visible, qualitative evidence to the difference in velocities.*

quared displacement) plotted against time for 0% and 1% biotin surface and $\alpha = 1.25$ for 0% biotin surface. *a. Mean squared displacement for one particle's trajectory for each surface. b. Mean squared displacement for 100 particles showing a linear relationship for each surface. c. The mean squared displacement and velocity both for the 0% and 1% biotin surface. d. MSD plotted against time to give a linear relationship for 100 particles. e. The trajectories with a zoomed-in view of the first 100 ms giving visible, qualitative evidence to the difference in velocities.*

To analyze *Figures 11* and *12*, we plot the mean squared displacement (MSD) against time. Particle tracking using MSD can provide information about the motion. MSD can be considered to be a measure of the distance traveled and described mathematically by $\langle \Delta r^2(\tau) \rangle = A\tau^\alpha$ where α is the MSD scaling exponent, which is the slope of the log-log plot of the time dependent MSD. The physical range of α is between 0 and 2. For random diffusion, MSD and time have a linear dependence and therefore $\alpha=1$ and for ballistic $\alpha=2$ (Gal *et al.*, 2013). Self-avoiding walk which describes the general movement of the DNA motor rollers, follows $\text{MSD} \sim t \log(t)$ where α lies between as shown in *Figure 13* (Yehl *et al.*, 2016).

provided basis for understanding the following line of simplifications to the particle's movement. The mechanisms driving the particle's motion are not yet clear, but the article has "explored" the system

and described mathematically by $\langle \Delta r^2(\tau) \rangle = A\tau^\alpha$ where α is the MSD scaling exponent, which is the slope of the log-log plot of the time dependent MSD. The physical range of α is between 0 and 2. For random diffusion, MSD and time have a linear dependence and therefore $\alpha=1$ and for ballistic $\alpha=2$ (Gal *et al.*, 2013). Self-avoiding walk which describes the general movement of the DNA motor rollers, follows $\text{MSD} \sim t \log(t)$ where α lies between as shown in *Figure 13* (Yehl *et al.*, 2016).

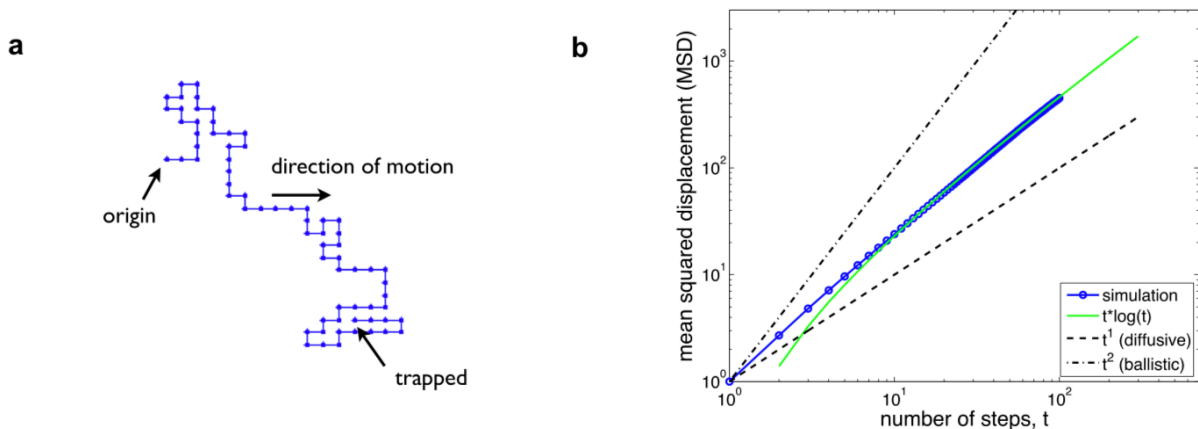


Figure 1 **a.** Trajectory for single self-avoiding walk.¹³ **b.** MSD vs. time (t) plot for 1000 particles: showing ballistic, diffusive and self-avoiding walk trends. At sufficiently long times, the simulation follows the expectation for self-avoiding walk, $MSD \sim t \log(t)$.¹

However, in my experiments, α did not equal 1 and was 1.56 at optimal rolling with conventional (0% biotin) particles and 0.5 with 100% biotin particles, both in the presence of streptavidin as shown in Figure 11. Therefore, the particle movement was not due to random diffusion and, rather, could best be described as self-avoiding movement. Additionally, Gal *et al.* describes the range of $0 \leq \alpha \leq 1$ as a non-active fluid, sub-diffusive motion, with extremes describing elastic (trapped) and viscous (diffusive) limits respectively. An α value in between these two extremes indicates obstruction to the particle's movement (Gal *et al.*, 2013). The value of $\alpha=0.5$ for the 100% biotin particles on a 1% surface thereby suggests the extreme hindrance the particles underwent in response to such a higher likelihood of biotin-streptavidin interaction.

The mean velocity and final displacement of the 0% biotin particles on a 1% biotin surface (1.98 $\mu\text{m/s}$ and 4.20 μm respectively) were significantly higher than that for the 100%

biotin particles (1.53 $\mu\text{m/s}$ and 2.11 μm respectively). This suggested that the particle's motion is not just as a result of random diffusion and that the concentration of biotin on the particle is inversely related to both the speed of the particle. Additionally, *Figure 12* suggests that increasing the concentration of biotin on the surface may also hinder movement as shown by the higher mean for the final displacement and velocity for the 0.1% biotin surface, 3.93 μm and 1.98 $\mu\text{m/s}$ respectively. This data thereby suggested that increasing the concentration of biotin on the surface and on the particle, both deter particle movement.

Following imaging of the particles, epifluorescence images were taken to confirm that particles actually rolled. Particles could move if they were not stuck to the surface and underwent random Brownian motion. Therefore, these depletion tracks lend clear evidence that the particles did, in fact, roll on the surface. The darker marks (depletion tracks) shown in *Figure 14* resulted from the RNase H cleavage of Cy3 fluorescently tagged RNA at these places. The train track-like mark shown in the image on the left resulted from the dimerization of particles. Yehl *et al.* found that about 1-10% of particles fuse forming dimers. They are a common byproduct in silica particle synthesis, and travel linearly and faster than single particles as suggested in the image with its common characteristic long two straight line marking (Yehl *et al.*, 2016).

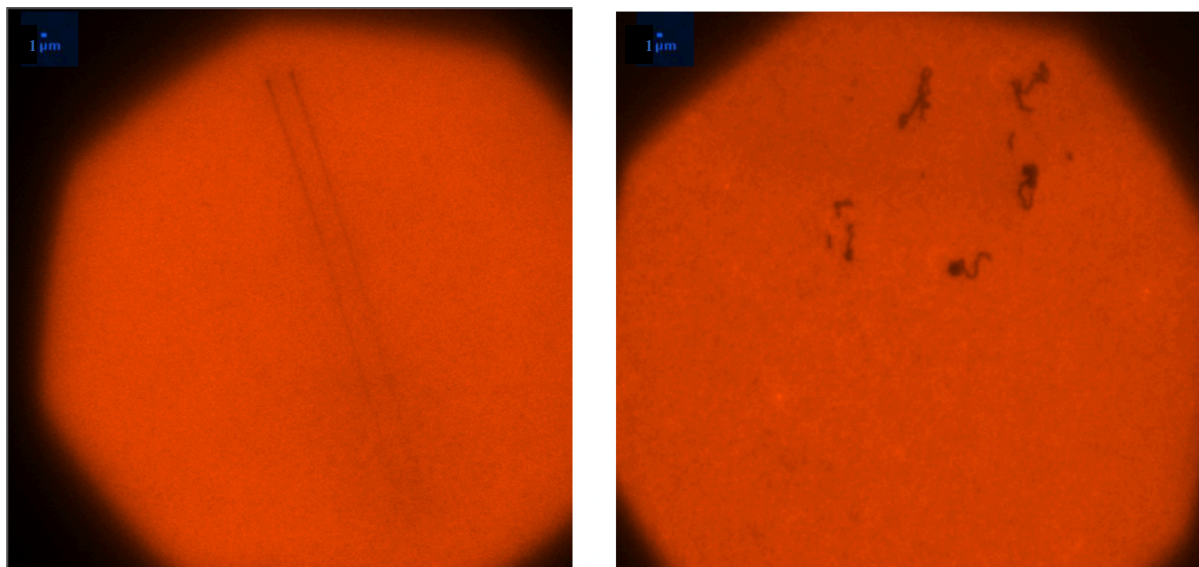


Figure 14. Depletion Tracks; dimer track (left) and typical, single particle track (right).

As addressed in the methods section, the next experiments were performed with streptavidin on the particle rather than on the surface. Particles functionalized with 100% biotin were incubated overnight with 0, 0.03, 0.1, 0.3, 1, 3 and 100 nM streptavidin and placed atop a surface with 25% biotin, yielding the results shown in *Figures 15* and *16*. The graph suggests that at 0, 0.03 and 0.3 nM streptavidin there was minimal hindrance. There was maximal hindrance at concentrations 1, 3 and 100 nM, and some particles were slowed at 0.1 nM. It appeared that at 1, 3 and 100 nM, there was full saturation as their average displacement curves are practically indiscernible and suggest minimal movement. These findings are congruent with the streptavidin fluorescence calibration produced in *Figure 9*, which shows clear saturation at 10 and 100 nM.

The aliquot of Triton used in this experiment was later found to be of lower concentration as it was measured by volume rather than mass as Triton has a soapy consistency

and therefore creates many air bubbles during pipetting. Therefore, ultimately the experiments, with a lower Triton concentration, yielded a more sensitive system than that in Figure 16.

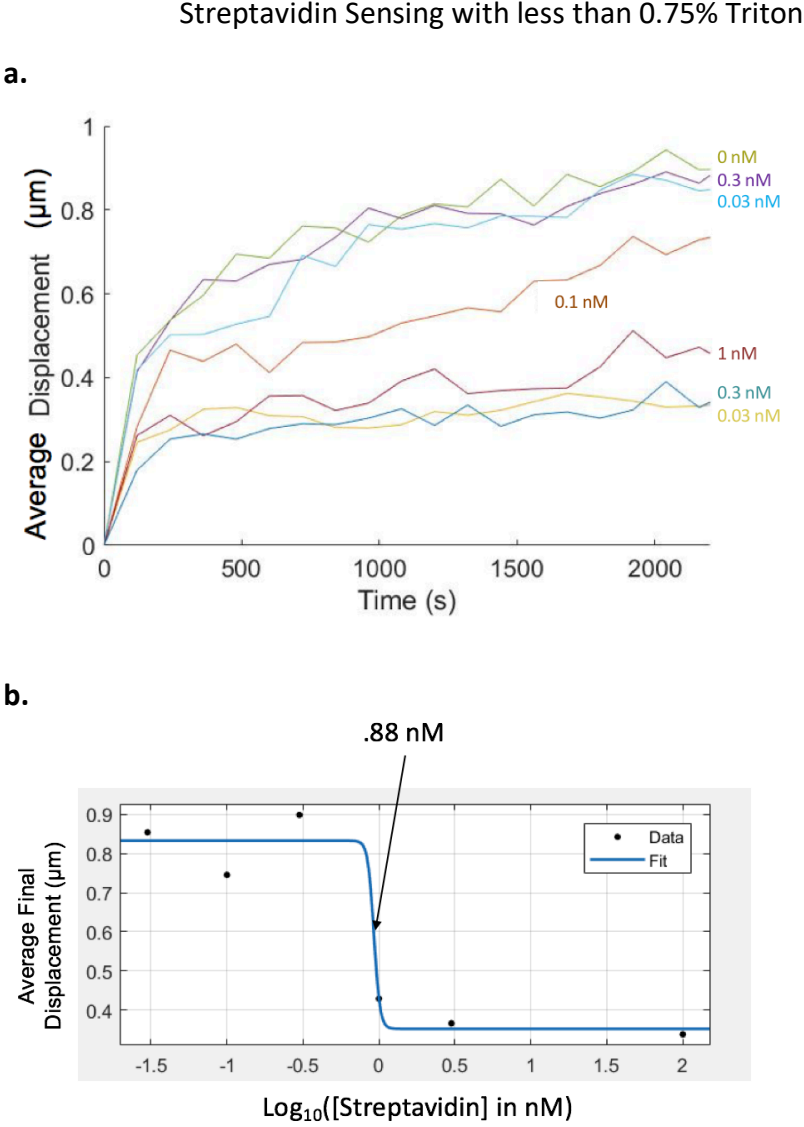


Figure 15. **a.** Average final displacement (μm) plotted against the log of streptavidin concentration for varying streptavidin concentration on 100% biotinylated particles on a 25% biotin surface. **b.** Average final displacement (μm) plotted over time for varying streptavidin concentration on 100% biotinylated particles on a 25% biotin surface.

Figure 15b shows a best fit curve suggesting that the velocity of the particles was slowed by half at a streptavidin concentration of 0.88 nM. The concentration values about this point show a steep decline in average final displacement suggesting that the system is most sensitive in detecting streptavidin in this range. Above those values suggest a total saturation of the biotin surface with streptavidin and therefore increasing the streptavidin concentration above 1 nM doesn't seem to make much of a difference to the particle displacement.

To combat an inaccurate dilution of Triton X, it was weighed for more precise measurements to the concentration of 0.75% used in previously conducted experiments (Gal *et al.*, 2015). However, based on the results shown in Figure 16, although the particles were faster overall, the system was far less sensitive. These results provided insight to the benefits of decreasing the Triton concentration.

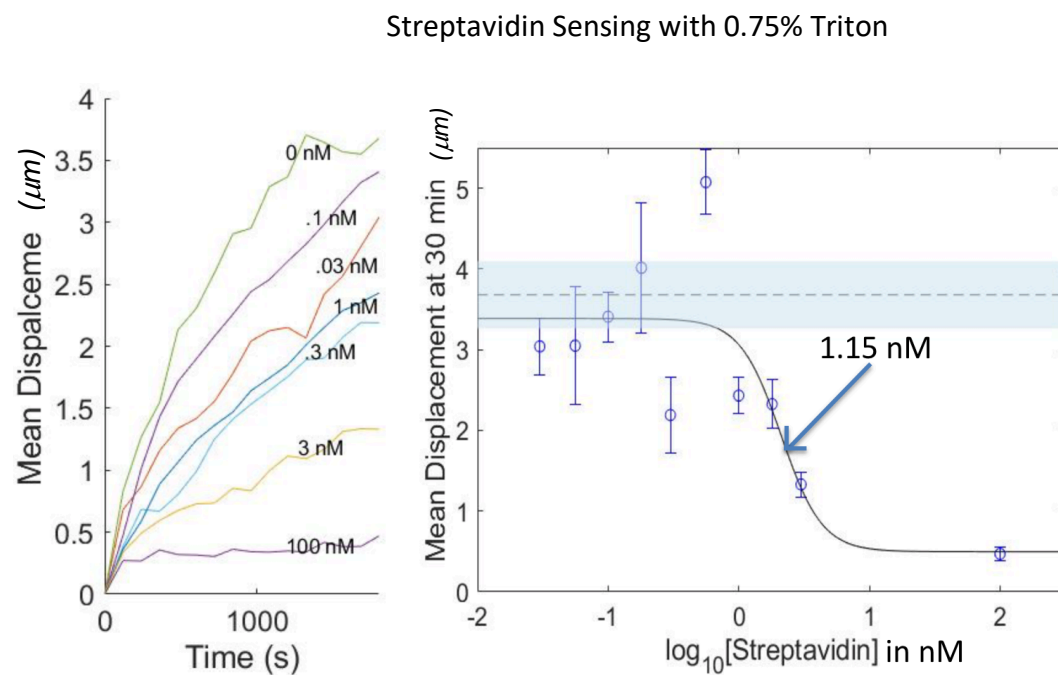


Figure 16. Varying streptavidin concentration on 100% biotinylated particles.

To truly compare and analyze the impact of Triton, an experiment was then conducted with one surface receiving 0.75% Triton and the other 0.1% Triton, shown in *Figure 17*. For the surface done with 0.1% Triton, there is a stark decrease in mean displacement from 1 nM to 3 nM streptavidin whereas the 0.75% Triton surface doesn't show a drop. Furthermore, 0.75% Triton still showed minimal sensitivity to streptavidin even at 100 nM.

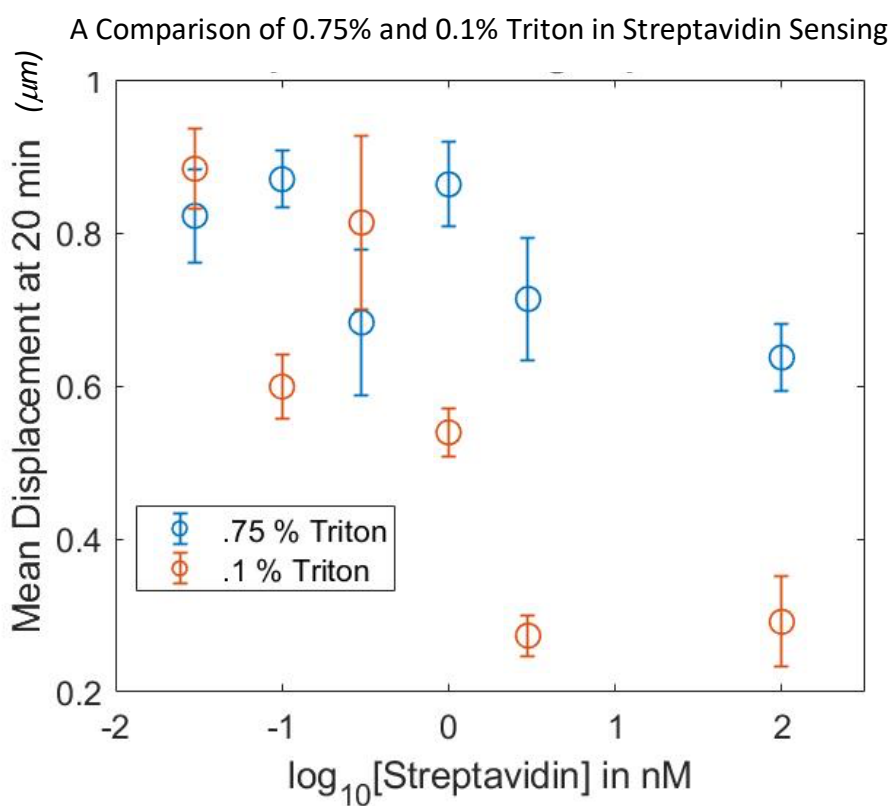


Figure 17. Triton concentration effect on sensitivity of the particle rolling to streptavidin concentration.

4. Conclusion and Future Directions

These experiments suggest that the DMW can function as an accurate sensing system. Additionally, the alteration of Triton X concentration used in the rolling solution to that used in previous literature suggests a means to further enhance the sensitivity of the DNA monowheel system. The multitude of data suggesting the decrease in velocity with increasing concentrations of streptavidin gives way to the inclusion of more clinically relevant proteins.

Hong *et al.* provides some potential clinical applications for this system. My current experiments use the DNA-base rolling motors to detect streptavidin but could be extended to aptamers to be applied to clinical diagnostics. Aptamers (aptasensors) are artificial nucleic acid ligands possessing specific binding characteristics to their targets. Several aptamers have been generated with high-affinity and specificity to numerous types of target molecules such as peptides, proteins, small organics, whole cells and toxic targets. Aptasensors can be used to identify biomarkers for cancer screening and detection of infectious microorganisms. Hong *et al.* describe that there is an increasing need for more sensitive, time-efficient and cost effective clinical tests as current methods are either too time consuming or expensive. Additionally, aptasensors can be used to detect diseases earlier using them to analyze body fluids such as blood and urine. This is crucial for increasing the chances of survival in cancer patients (Hong *et al.*, 2012).

Table 3, taken from the article, shows the numerous ways in which aptamers can be used to detect various cancer markers using a diverse array of detection methods, such as the sandwich conjugate modified electrode which uses DNA labeled with biotin. This method was

of particular interest as it utilizes a system similar to the experiments previously outlined and discussed.

Table 3: Using aptamers to detect various forms of cancer ⁶

Cancer marker detected	Aptamer	Detection type	Signal transduction	Linear range/LOD	Reference
HeLa cells, K562 cells, MDA-231 cells	DNA	Label free detection	Electrochemical	n.s./n.s.	Feng <i>et al.</i> (2011) [39]
PDGF-BB	DNA labeled with biotin	A sandwich conjugate modified electrode	ECL	1.0×10^{-13} to 1.0×10^{-11} M/ 2.7×10^{-14} M	Chai <i>et al.</i> (2011) [40]
Ramos cancer cell, CEM cells	DNA	ECL array with a novel cycle-amplifying technique	ECL	n.s./n.s.	Jie <i>et al.</i> (2011) [41]
Multi-marker or Ramos cells, CCRF-CEM cells, Toledo Cells	DNA-conjugated FRET NP	Simultaneous multiplexed analysis	fluorescence	n.s./n.s.	Chen <i>et al.</i> (2009) [42]
Ramos cancer cell	DNA	Label free detection	ECL	100 to 1,000 cells mL ⁻¹ /58 cells mL ⁻¹	Hun <i>et al.</i> (2011) [43]
Leukemia cells	DNA conjugated apt-MBs	a magnet-quartz crystal microbalance system	QCM	1×10^4 to 1.5×10^5 cells mL ⁻¹ / 8×10^3 cells mL ⁻¹	Pan <i>et al.</i> (2010) [44]
PSA	DNA labeled with FITC	Aptamer blotting assay	Chemiluminescence	40 to 100 nM/n.s.	Savory <i>et al.</i> 2010 [45]
MUC1	DNA labeled with single PPy nanowire-based microfluidic	One step electrochemical deposition method	Electrochemical	n.s./2.66 nM	Huang <i>et al.</i> (2011) [33]
MUC1	DNA labeled with QD	Aptamer-based detection with quantum-dot based fluorescence readout	Fluorescence	n.s./250 nM	Cheng <i>et al.</i> (2009) [46]
GSH	RNA	SPR analysis and isocratic affinity chromatography	SPR	n.s./n.s.	Bala <i>et al.</i> (2011) [47]
VEGF	RNA conjugated CPNTs	FET-type biosensor based on CPNTs-aptamer	Electrochemical	n.s./400 fM	Kwon <i>et al.</i> (2010) [48]

In blood cells, plasma proteins or free DNA may be markers of a tumor. Platelet-derived growth factor B chain (PDGF-BB) is a potential marker of tumor growth. Chai *et al.* developed a ECL aptasensor for PDGF-BB as shown in *Figure 18*. First, the biotinylated aptamer nanoprobe were immobilized on a streptavidin coated gold nanoparticle (AuNPs) and then PDGF was bound to the aptamers. Lastly, the labeled aptamer signal probes, ABEI-AuNPs, was bound to the PDGF-BB forming a sandwich conjugate modified electrode (Chai *et al.*, 2011). The scheme currently used in the biotin and streptavidin experiments could be extended to cancer testing

like that used in this experiment by functionalizing the surface with PDGF and the particle with the aptamer.

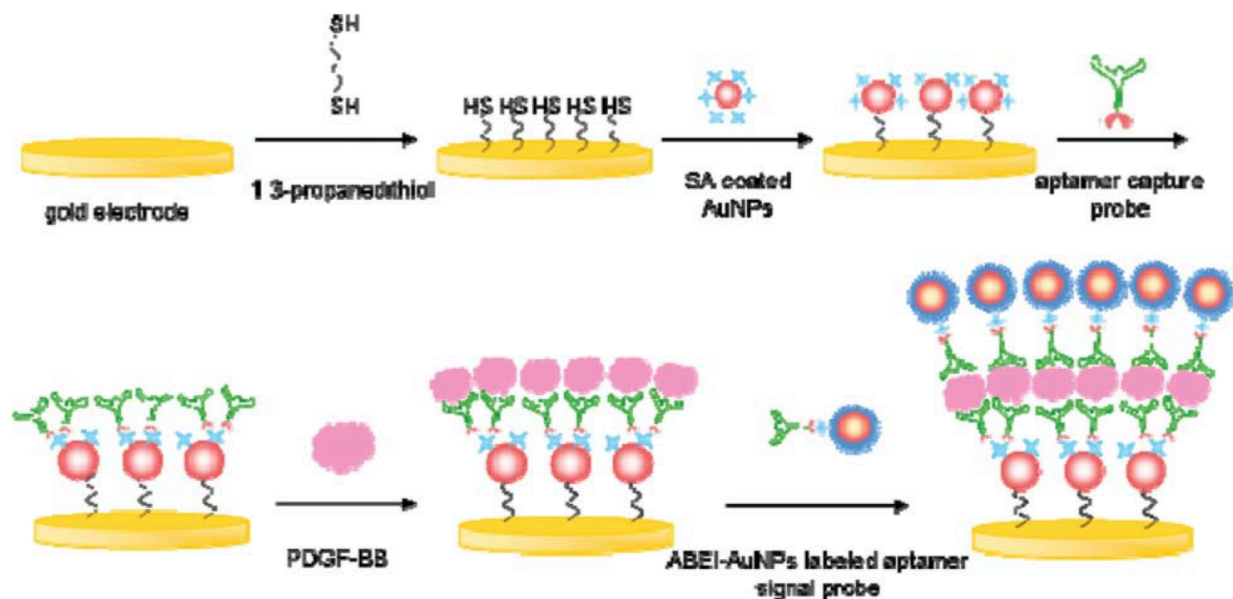


Figure 18. A sandwich conjugate modified electrode modified with streptavidin coated particles which binds biotinylated aptamers. These aptamers detect and bind PDGF-BB, which is a marker of tumor growth whose concentration can in turn be detected via the binding of an ABEI-AuNPs labeled aptamer signal probe.³

This DNA motor system gives way to a multitude of possibilities. Taking advantage of the known strong interaction between biotin and streptavidin in these experiments, the system could be fine-tuned to enhance sensitivity and particle speed. In future experiments, the implementation of various aptamers with medical significance could lead to great breakthroughs in early disease detection and, therefore, improved survival rates.

5. References

1. Bath, Jonathan, Simon J. Green, and Andrew J. Tuberfield. "A Free-Running DNA Motor Powered by a Nicking Enzyme." *Chem. Int. Ed.*, 2005, 44 (28), 4358–4361.
2. "Biotin Oligonucleotide Modification." *Bio-Synthesis Inc*, Oligonucleotides, n.d.
3. Chai, Y., J. Gu, and H. Cui. "A Novel Electrochemiluminescence Aptasensor for Protein Based on a Sensitive N-(Aminobutyl)-N-Ethylisoluminol-Functionalized Gold Nanoprobe." *Analyst*, 2011.
4. Fang, S., H. J. Lee, A. W. Wark, H. M. Kim, and R. M. Corn. "Determination of Ribonuclease H Surface Enzyme Kinetics by Surface Plasmon Resonance Imaging and Surface Plasmon Fluorescence Spectroscopy." *Analytical Chemistry*, 2005.
5. Gal, Naama, Diana Lechtman-Goldstein, and Daphne Weihs. "Particle Tracking in Living Cells: A Review of the Mean Square Displacement Method and Beyond." *Rheologica Acta* 52, no. 5 (2013): 425–43.
6. Hong, P., W. Li, and J. Li. "Applications of Aptasensors in Clinical Diagnostics." *Sensors, Aptamer-Based Sensors*, 12(2) (2012): 1181–93.
7. Kassem, S., T. van Leeuwen, A. S. Lubbe, M. R. Wilson, B. L. Feringa, and D. A. Leigh. "Artificial Molecular Motors." *Chem. Soc. Rev.* 46 (9) (2017): 2592–2621.
8. Lodish, Harvey, Arnold Berk, Lawrence S. Zipursky, Paul Matsudaira, David Baltimore, and James Darnell. "Molecular Cell Biology." In *Myosin: The Actin Motor Protein*, 4th ed. 18.3. W. H. Freenab and Company, 2000.
9. Lund, K., A. J. Manzo, N. Dabby, N. Michelotti, A. Johnson-Buck, J. Nangreave, S. Taylor, et al. "Molecular robots guided by prescriptive landscapes." *Nature* 465 (7295) (2010): 206–10.

10. Omabegho, T., R. Sha, and N. C. Seeman. "A Bipedal DNA Brownian Motor with Coordinated Legs." *Science* 324 (5923) (2009): 67–71.
11. Sun, Junling, Yilei Wu, Zhichang Liu, Dennis Cao, Yuping Wang, Chuyang Cheng, Dongyang Chen, Michael R. Wasielewski, and Fraser J. Stoddart. "Visible Light-Driven Artificial Molecular Switch Actuated by Radical–Radical and Donor–Acceptor Interactions." *ACS Publications, The Journal of Physical Chemistry*, 2015, 6317–25.
12. Weber, P. C., D. H. Ohlendorf, J. J. Wendoloski, and F. R. Salemme. "Structural Origins of High-Affinity Biotin Binding to Streptavidin." *Science* 243, no. 4887 (1989): 85–88.
13. Yehl, K., A. Mugler, S. Vivek, Y. Liu, Yun Zhang, M. Fan, E. R. Weeks, and K Salaita. "High-Speed DNA-Based Rolling Motors Powered by RNase H." *Nat. Nanotechnol.* 11 (2) (2016): 184–90.